

VOLUME-FILLING AND QUORUM-SENSING IN MODELS FOR CHEMOSENSITIVE MOVEMENT

KEVIN J. PAINTER AND THOMAS HILLEN

ABSTRACT. Chemotaxis is one of many mechanisms used by cells and organisms to navigate through the environment, and has been found on scales varying from the microscopic to the macroscopic. Chemotactic movement has also attracted a great deal of computational and modelling attention. Some of the continuum models are unstable in the sense that they can lead to finite time blow-up, or “overcrowding” scenarios. Cell overcrowding is unrealistic from a biological context, as it ignores the finite size of individual cells and the behaviour of cells at higher densities. We have previously presented a mathematical model of chemotaxis incorporating density dependence that precludes blow-up from occurring, [19]. In this paper, we consider a number of approaches by which such equations can arise based on biologically realistic mechanisms, including the finite size of individual cells - “volume filling” and the employment of cell density sensing mechanisms - “quorum-sensing”. We show the existence of nontrivial steady states and we study the traveling wave problem for these models. A comprehensive numerical exploration of the model reveals a wide variety of interesting pattern forming properties. Finally we turn our attention to the robustness of patterning under domain growth, and discuss some potential applications of the model.

1 Introduction An essential characteristic of living organisms is the ability to sense signals in the environment and adapt their movement accordingly. This allows the location of food, the avoidance of predators or the search for mates. When the response involves the detection of a chemical, it is termed *chemotaxis*, *chemokinesis*, or generally *chemosensitive movement*. The term *chemotaxis* is used broadly in the mathematical literature to describe general chemosensitive movement responses, and it is in this context that we use the term here. However, it is important to bear in mind that this definition has a more

AMS subject classification: 92C17, 92C15.

Copyright ©Applied Mathematics Institute, University of Alberta.

restricted use in the experimental community (see also the discussion in [18]). Chemotaxis can be either positive (chemoattraction) or negative (chemorepulsion).

Models for chemotaxis have been successfully applied to bacteria, slime molds, skin pigmentation patterns, leukocytes and many other examples. Independent of the species at hand, the basic features of chemotactic movement can be formulated in relatively straightforward models.

In this paper we study the following model for chemotactic movement

$$(1) \quad \begin{aligned} \frac{\partial u}{\partial t} &= D_u \nabla^2 u - \nabla \cdot \{u\chi(u, v)\nabla v\} + f(u, v) \\ \frac{\partial v}{\partial t} &= D_v \nabla^2 v + g(u, v), \end{aligned}$$

where $u(x, t)$ represents the density of the cell-population, and $v(x, t)$ represents the chemoattractant (repellent) concentration. The chemotactic component is represented by the negative-cross diffusion term in the cell density equation, where $\chi(u, v)$ is commonly referred to as the *chemotactic sensitivity*. Cell and chemical kinetics are given by f and g respectively. In applications, typically zero-flux boundary conditions on a bounded domain in \mathbb{R}^n are applied.

In an extension to earlier works on Keller-Segel type of models we consider cross-diffusion terms of the form $u\chi(u, v)\nabla v$, compared to $u\chi(v)\nabla v$ in classical applications. Thus, the population density of the chemotacting population directly modulates its own sensitivity response. For the specific form $u(1-u)\chi(v)\nabla v$, in [19] we have shown that this change leads to global existence of solutions (independent of space dimension) and to pattern formation.

In Section 2, we review some of the basic literature on chemotaxis. In Section 3, we derive models based on realistic biological assumptions, which incorporate the effects of *volume filling* and *quorum sensing* mechanisms and lead to the form of equation given by Equations (1). We analyse the structure of the steady states. In Section 4 we analytically and numerically study the travelling wave problem for (1). In Section 5 we explore the tremendous variety in pattern formation. In Section 6 we look at the effect of domain growth on the patterning. Finally, we discuss some potential applications of the model, however the detailed modelling should be carried out elsewhere.

2 Chemosensitive movement Chemosensitive movement has been shown to play an integral role in cell guidance and tissue organisa-

tion during embryonic growth. The early wiring of the nervous system crucially depends on the detection and response to a group of chemical cues by the tip of the growing nerve cells (growth cone), [59]. By acting as attractants to some nerve types, while repelling others, the chemicals help mediate the finely tuned movements required to form trillions of connections. Chemotaxis has also been postulated to play a role in cell guidance of other developmental process, such as primitive streak guidance [65] and limb-bud patterning [30].

Cell-chemotaxis is also crucial during the subsequent physiological maintenance of an organism: for example, the guidance of immune cells to targets is mediated through chemotaxis. In tumour growth, the stimulation of new blood vessel growth (“angiogenesis”), mediated by chemotaxis, is an indicator of increased malignancy. At a macroscopic level, chemotactic-type responses allow sharks to detect blood in the water many miles from a wounded animal, while moths emit pheromones as a mechanism for attracting mates.

The greatest understanding into the mechanisms for these movements have resulted from studies of chemosensitive movement in bacteria such as *Escherichia coli* and *Salmonella typhimurium*. *E. coli* moves via rotation of flagella and, when rotating anticlockwise, these flagella bundle together resulting in a period of smooth swimming - a “run”. Clockwise rotation, however, results in the flagella spraying outwards resulting in a random reorientation, or a “tumble”. Normal swimming is characterised by periods of smooth runs punctuated by tumbling. In the presence of a chemoattractant, *E. coli* bias their behaviour by tumbling less frequently in an increasing attractant gradient, resulting in the general movement towards high concentrations. Detection of the attractant is made by the binding of attractant molecules to cell surface receptors, which subsequently initiates a cell internal pathway which transduces the signal to the movement machinery, [1].

In other bacteria or in eukaryotic cells the movement mechanism can be substantially different. In the cellular slime mold, *Dictyostelium discoideum*, the sensing of a chemotactic signal (*cAMP*) invokes the protrusion of a pseudopod at the point of detection and subsequent elongation of the cell body. Adhesion to the substrate takes place at the front of the cell, and loss of adherence at the cell rear permits forward movement of the cell, (e.g., see [16, 10]).

In modelling chemosensitive movement, increased computational power has allowed the greater employment of approaches where cells are treated as individuals (see e.g. [46, 12]). Other approaches employ continuum-based models, in particular the Patlak-Keller-Segel type sys-

tems ([**26**, **47**):

$$\begin{aligned}\frac{\partial u}{\partial t} &= D_u \nabla^2 u - \nabla \cdot \{u\chi(v)\nabla v\} + f(u, v) \\ \frac{\partial v}{\partial t} &= D_v \nabla^2 v + g(u, v)\end{aligned}$$

For suitable kinetics, the above model has been shown to demonstrate pattern forming properties, with cells accumulating into high density aggregations. The simplicity of the above model has resulted in extensive application in a number of biological systems, including aggregation patterns in bacteria [**62**, **63**, **64**], fish skin pigmentation patterning [**45**] and angiogenesis in tumour progression and wound healing ([**9**, **40**, **48**]). The model has also attracted a great deal of mathematical analysis, in particular for the tendency of solutions to exhibit finite-time blow-up; for more information see the reviews of Horstmann [**20**, **21**].

Blow-up is undesirable from a biological standpoint, since it implies the formation of cell aggregates of infinite density. Furthermore, the highly stiff nature of the problem can create many difficulties from a computational standpoint. In Hillen and Painter [**19**], the chemotactic sensitivity depended additionally on the cell density, $\chi = \chi(u, v)$, such that:

- $\chi(0, v) > 0$.
- There exists a $\bar{u} > 0$ such that $\chi(\bar{u}, v) = 0$ and $\chi(u, v) > 0$ for $0 < u < \bar{u}$.

The simplest non-trivial choice is

$$\chi(u, v) = \chi_0(1 - u).$$

Intuitively, the above conditions result in a switch to repulsion at high densities, and thus we may expect a limit upon the size to which an aggregation can grow. This was proved rigorously in [**19**], where an invariant region for solutions was shown, and solutions initiating within this region were shown to exist globally in time. Numerical simulations demonstrated aggregation, where the density to which aggregations could grow was controlled. For typical patterns see Figure 5 later in this paper.

Density-dependence in the motility may arise via a wide range of processes. Simply, the ability of a cell to migrate will be partially dependent on the availability of space within its environment. Secondly, cellular

adhesion, involving the contact and attachment between neighbouring cells via classes of extracellular receptors, mediates cellular reorganisation and positioning within tissues. Thirdly, the secretion of external diffusible substances, allows cells to intercommunicate, mediating a wide variety of processes including migration responses.

3 Derivation of chemotactic equations Throughout the derivations of the chemotaxis models in this section we neglect cell proliferation and cell deaths, hence $f(u, v) = 0$. Later we include f as an additional term, which incorporates the assumption that the oriented movement and the cell kinetics are independent processes which act on similar time scales.

To derive models for chemotaxis, we use the approach of Othmer and Stevens (for more details, see [41] and the reference therein), where a master equation for a continuous-time, discrete-space random walk on a one-dimensional equi-distant lattice is considered. We define $u_i(t)$ to be the probability of a walker to be at $i \in \mathbf{Z}$ at time t , conditioned on beginning at $i = 0$ at $t = 0$. We assume this evolves according to the continuous-time discrete-space equation:

$$(3) \quad \frac{\partial u_i}{\partial t} = \mathcal{T}_{i-1}^+ u_{i-1} + \mathcal{T}_{i+1}^- u_{i+1} - (\mathcal{T}_i^+ + \mathcal{T}_i^-) u_i.$$

In the above $\mathcal{T}_i^\pm(\cdot)$ define the transitional-probabilities per unit time of a one-step jump to $i \pm 1$. Herein, we shall equate the probability distribution above with the cell density. The above model simply describes the changing particle/cell numbers as individuals enter or leave a site.

3.1 The classical chemotaxis model The dependence of the transitional probabilities, \mathcal{T}_i^\pm , is crucial on the form of equation we derive. In the context of chemosensitive movement, the decision of when/where to jump is dependent on additional factors, such as the external concentration of a chemotactic agent. This introduces a spatial bias into the random walk, and we therefore assume $\mathcal{T}_i^\pm = \mathcal{T}_i^\pm(v)$, where v is a vector representing the chemical concentration defined on the lattice. While a variety of different models can be postulated for how the cells detect the chemical concentration (see [41]), we assume here that cells have the capacity to detect a local gradient, i.e.,

$$(4) \quad \mathcal{T}_i^\pm = \alpha + \beta (\tau(v_{i\pm 1}) - \tau(v_i))$$

where α and β are constants and τ represents the mechanism of signal detection. The ratio of α to $\beta(\tau(v_{i\pm 1}) - \tau(v_i))$ models the strength of

random motility to chemotaxis. For transitional probabilities of this form (4) we always assume that they are not negative; that is, α is not small compared to β and the variations $\tau(v_{i\pm 1}) - \tau(v_i)$ are not too large.

We substitute (4) into Equation (3), which under rearrangement gives:

$$\begin{aligned} \frac{\partial u_i}{\partial t} &= \alpha(u_{i+1} - 2u_i + u_{i-1}) \\ &\quad - \beta((u_{i+1} + u_i)(\tau(v_{i+1}) - \tau(v_i)) - (u_i + u_{i-1})(\tau(v_i) - \tau(v_{i-1}))) \end{aligned}$$

We set $x = ih$, reinterpret x as a continuous variable and extend the definition of u_i accordingly. As the spatial scale, h , is changed, the transitional probabilities to jump to a neighbouring location must depend on that scale. Thus we assume that $\mathcal{T}_h^\pm = \frac{k}{h^2} \mathcal{T}^\pm$ for some scaling constant k . As we expand the right-hand side in powers of h we obtain for the density $u(x, t)$:

$$\frac{\partial u}{\partial t} = k \left(\alpha \frac{\partial^2 u}{\partial x^2} - 2\beta \frac{\partial}{\partial x} \left(u \frac{\partial \tau(v)}{\partial x} \right) \right) + \mathcal{O}(h^2).$$

In the limit of $h \rightarrow 0$ we formally arrive at the following model for chemotaxis:

$$\frac{\partial u}{\partial t} = D_u \frac{\partial^2 u}{\partial x^2} - \frac{\partial}{\partial x} \left(u \chi(v) \frac{\partial v}{\partial x} \right)$$

where

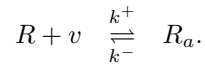
$$(5) \quad D_u = k\alpha, \quad \text{and} \quad \chi(v) = 2k\beta \frac{d\tau(v)}{dv}.$$

The above model is of the same form originally proposed by Patlak, [47] and Keller and Segel, [26]. The function $\chi(v)$ is commonly referred to as the *chemotactic sensitivity* function. The simplest assumption is a linear dependence for τ on v , in which case $\chi = \chi_0$ is constant. For this sensitivity, we add cell and chemical kinetics of the form $f(u, v)$ and $g(u, v)$ respectively, and we extend to higher dimensions:

$$(6) \quad \begin{aligned} \frac{\partial u}{\partial t} &= D_u \nabla^2 u - \chi_0 \nabla \cdot \{u \nabla v\} + f(u, v) \\ \frac{\partial v}{\partial t} &= D_v \nabla^2 v + g(u, v) \end{aligned}$$

where D_v is the chemical diffusion coefficient. We shall refer to this model as the “classical chemotaxis equation”. It is also possible to incorporate details of the process of signal detection and transduction by

the cells. For example, as outlined in the introduction, chemoattractant detection in *E. coli* involves the binding of molecules to cell surface receptors, subsequently initiating a complex pathway linking to a movement response. We assume that the binding of the chemical v to a cell receptor R converts it into an active form R_a according to:



If (1) binding and disassociation occur on a much faster timescale than subsequent signal transduction, and (2) the total number of cell surface receptors, R_0 , remains about constant, then the number of activated receptors is $R_a = R_0 v / (K + v)$, $K = k_- / k_+$. Assuming the chemotactic response relates to the number of occupied receptors, $\tau(v) \propto R_a$ then we obtain a receptor response law, [55]:

$$\chi(v) = \frac{\rho}{(K + v)^2}.$$

where ρ is a constant.

Equations (6) have been studied for various forms of f and g . In particular, for chemical kinetics of the form $g(u, v) = u - v$, the model has been shown to give rise to spatial patterning phenomena. In two or higher dimensions, this can take the form of finite time blow-up (see references in [20, 21]). Blow-up explains the initial aggregation, but is problematic from the biological viewpoint, since it implies the formation of aggregations of infinite cell density. Furthermore the highly stiff problem creates restrictions on numerical evaluation of the model. It is therefore desirable to develop simple models for chemotaxis in which blow-up behaviour is precluded and solutions exist globally.

We extend the derivation of the above model to incorporate two potentially important factors: (1) The effect of the finite volume of the organism on the ease of movement, and (2) The effect of chemical-mediated cell density sensing mechanisms on movement.

3.2 Volume-filling chemotaxis models In the volume filling approach, we assume that the probability of making a jump depends upon the availability of space into which it can move. For example, consider Figure 1(a) where cells (circles) are chemotactically migrating in an increasing attractant gradient. Cell A is in a low density region, and can move with freedom, though the chemosensitive bias is to the right. Cell B, on the other hand, is in a semi-packed environment and although it

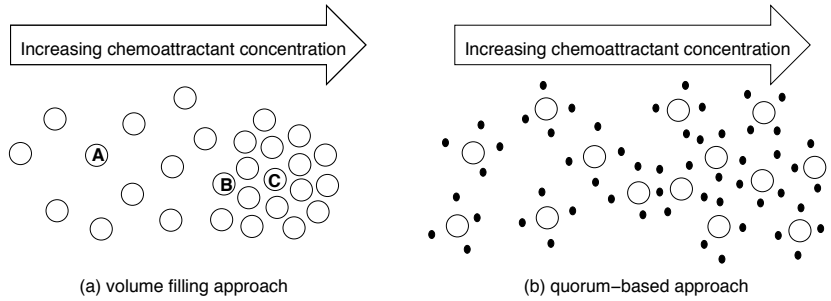


FIGURE 1: Illustration of the (a) Volume filling model, and (b) Quorum sensing model

experiences a bias to the right, the lack of space inhibits motion in that direction. Cell C is completely packed on all directions, and unable to move.

We incorporate this into the derivation of a chemotaxis equation by assuming that the probability of jumping into a neighbouring site is dependent upon the amount of space available at that site, i.e.,

$$(7) \quad \mathcal{T}_i^\pm = q(u_{i\pm 1})(\alpha + \beta(\tau(v_{i\pm 1}) - \tau(v_i)))$$

where $q(u)$ is the probability of the cell finding space at its neighbouring location. We shall assume that only a finite number of cells, U_{\max} , can be accommodated at any site, and thus we stipulate the following conditions on q :

$$q(U_{\max}) = 0 \text{ and } q(u) \geq 0 \text{ for all } 0 \leq u < U_{\max}$$

Clearly, a logical choice is

$$q(u) = 1 - \frac{u}{U_{\max}},$$

which states that the probability of a jump into a site decreases linearly with the cell density at that site. A more complex choice could incorporate other cellular processes, e.g.

$$q(u) = u \left(1 - \frac{u}{U_{\max}} \right).$$

This models a biphasic response; at low cell densities the probability of a jump increases with cell density, while at high densities the probability

decreases with cell densities. The response at low densities may arise through the necessity of cellular contact for migration to occur.

Substituting Equations (7) in to the Master Equation (3) gives:

$$\begin{aligned} \frac{d}{dt}u_k &= q_k(\alpha + \beta(\tau_k - \tau_{k-1}))u_{k-1} + q_k(\alpha + \beta(\tau_k - \tau_{k+1}))u_{k+1} \\ &\quad - \left(q_{k+1}(\alpha + \beta(\tau_{k+1} - \tau_k)) + q_{k-1}(\alpha + \beta(\tau_{k-1} - \tau_k)) \right) u_k \\ &= \alpha \left(q_k u_{k-1} + q_k u_{k+1} - (q_{k+1} + q_{k-1}) u_k \right) \\ &\quad + \beta \left(q_k (\tau_k - \tau_{k-1}) u_{k-1} + q_k (\tau_k - \tau_{k+1}) u_{k+1} \right. \\ &\quad \left. - q_{k+1} (\tau_{k+1} - \tau_k) u_k - q_{k-1} (\tau_{k-1} - \tau_k) u_k \right). \end{aligned}$$

Once more, we reinterpret space as a continuous variable and expand the right hand side. In the limit, we arrive at the PDE:

$$\frac{\partial u}{\partial t} = k\alpha \left(q(u) \frac{\partial^2 u}{\partial x^2} - u \frac{\partial^2 q(u)}{\partial x^2} \right) - 2k\beta \frac{\partial}{\partial x} \left(q(u) u \frac{\partial \tau(v)}{\partial x} \right)$$

which in divergence form reads:

$$(8) \quad \frac{\partial u}{\partial t} = \frac{\partial}{\partial x} \left(D_u (q(u) - q'(u)u) \frac{\partial u}{\partial x} - q(u)u\chi(v) \frac{\partial v}{\partial x} \right)$$

where $q'(u)$ denotes the derivative of q with respect to its argument, and D_u and $\chi(v)$ are given by (5). Note that for non-increasing $q(u)$ the diffusion coefficient $D_u(q(u) - q'(u)u)$ is always positive, hence (8) is well defined.

Including cell kinetics and signal dynamics we arrive at a model for chemosensitive movement incorporating volume filling:

$$(9) \quad \begin{aligned} \frac{\partial u}{\partial t} &= \frac{\partial}{\partial x} \left(D_u (q(u) - q'(u)u) \frac{\partial u}{\partial x} - q(u)u\chi(v) \frac{\partial v}{\partial x} \right) + f(u, v) \\ \frac{\partial v}{\partial t} &= D_v \frac{\partial^2 v}{\partial x^2} + g(u, v) \end{aligned}$$

For the special choice of $q(u) = 1 - u/U_{\max}$ we obtain $q(u) - q'(u)u = 1$. For this choice of q we study the relative density $\tilde{u} = u/U_{\max}$, (and drop the $\tilde{\cdot}$). Combined with chemical dynamics and cell kinetics and extended

to general dimensions we finally get system (1) with $\chi(u, v)$ replaced by $\chi(v)(1 - u)$.

With chemical kinetics of the form $g(u, v) = g_1(u, v)u - g_2(u, v)v$ and $f(u, v) = 0$, the above model (1), was previously introduced in [19] where it has been shown that all solutions of this model (and generalisations) exist globally in time and there is no finite time blow-up. Intuitively, this is what we would expect from a “volume-filling” approach: cells aggregate into a space until maximum capacity is reached, after which no more cells can move in.

Other choices for $q(u)$ can also be considered, for example, if we choose

$$q(u) = 1 - u^\gamma, \quad \gamma \geq 0$$

then $q(u) - q'(u)u = 1 + (\gamma - 1)u^\gamma$. This gives, compared to diffusion without volume filling mechanism, enhanced diffusion for $\gamma > 1$ and reduced diffusion for $\gamma < 1$.

3.3 “Quorum-sensing” approaches The volume-filling approach provides an intuitive way into how density-dependent chemotactic models may be realistically derived. In most tissues, however, the cell density is carefully controlled at levels well below the theoretical maximum resulting from tight packing. Excessive cell densities may result in over-depletion of important nutrients and necrosis, as occurs in pathological diseases such as cancer.

While the mechanisms in place for this regulation are largely unknown, a great deal of interest has recently been generated by “quorum-sensing”, or population sensing, in bacterial populations [33, 56, 57]. A wide range of physiological processes in bacteria have been shown to depend on the bacterial population density. A well-studied example is the light generating marine bacteria *Vibrio fischeri*, which forms a symbiotic relationship with a number of eukaryotic hosts by providing light in exchange for nutrients [54]. The bacteria only start generating light at high cell densities, since low cell numbers produce insufficient light. Cells detect the population level by sensing the concentration of a diffusible chemical secreted into the environment, known as an “auto-inducer”. Light production is only stimulated when this is sufficiently high. Such “quorum-sensing” has been shown to induce a diverse range of physiological functions in many bacteria, including antibiotic secretion and bio-layer-formation in *Pseudomonas aeruginosa*, swarming motility in *Burkholderia cepacia* and sporulation in *Myxococcus xanthus* (see above references).

Similar mechanisms occur in eukaryotic populations. The cellular slime mold *Dictyostelium discoideum* has been widely studied due to its particular life-cycle. In a nutrient rich environment, the population grows while the amoeboid cells consume the available nutrient. Starvation, however, stimulates secretion of cAMP, inducing other *D. discoideum* cells both to secrete cAMP and chemotactically migrate towards the cAMP source, resulting in an aggregation. Cellular differentiation follows, eventually resulting in a fruiting body structure composed of a ball of spore cells supported by a stalk of dead cells. This positions the spore cells such that dispersion into a more favourable environment can occur. Quorum-sensing type behaviour occurs both prior to starvation and during aggregation stages. At starvation cells secrete CMF (*glyco-protein conditioned medium factor*) into the environment, and only when a sufficient concentration of CMF is detected do the cells start the cAMP pathway, [13]. This may ensure that the environment is sufficiently depleted of resources before the aggregation process is initiated. During aggregation, cells secrete another molecule, counting factor (CF), which regulates the size of the aggregation to optimise the efficiency with which the fruiting body can disperse the cells, [5, 6]. The CF is thought to determine the group size via modulation of the adhesive and motility properties of the cells [52].

Clearly, “quorum-sensing” behaviour may play a key role in regulating a huge variety of cell functions. We incorporate the effect of such a mechanism by assuming the existence of a secondary chemical which allows the cells to determine the local density and alter the chemotactic response to the chemoattractant v accordingly. For example, consider again Figure 1. In the volume filling approach, (a), cells aggregate until packed. However, if cells are also secreting a secondary molecule, (b), then the concentration of the molecules sensed by the cell will be an indicator of the local density. Response to the chemoattractant is regulated by the quorum sensing molecule, providing a mechanism by which cells can pack at a lower density. We therefore assume transitional probabilities of the general form, $\mathcal{T}_n^\pm(v, w)$, where v is the chemoattractant and w is the quorum-sensing molecule. Different models can be derived, depending on exactly how the quorum sensing modulates the signalling pathway. Here we consider two possibilities:

3.3.1 Mediating attractant strength We first assume that w modulates the sensitivity to chemical gradients, i.e.,

$$\mathcal{T}_n^\pm = \alpha + \beta(w_i) (\tau(v_{i\pm 1}) - \tau(v_i))$$

Again we assume that the parameters involved are such that $\mathcal{T}_n^\pm \geq 0$.

Here we are assuming that w is interfering with the chemotactic signalling pathway downstream of detection; i.e., cells sense the same gradient of chemical at the surface, but the “strength” signalled to the movement dynamics is modulated by w .

This may be an apt description of the response of growing nerve cells to a variety of molecules. Certain chemicals have been shown to elicit both attractant and repellent responses, depending on the environmental state of the neuron, e.g. [59, 58, 34]. In high concentrations of extracellular cAMP the response to Netrin-1 is attractive, while at lower cAMP levels the response is repellent. In the above, these responses may be modelled by choosing $\beta(w)$ such that $\beta(w) < 0$ for $w < w^*$ and $\beta(w) \geq 0$ for $w \geq w^*$. Dual responses of cells to single chemical agent have also been identified in chemotactically migrating mesoderm cells, [29] and immune cells [51].

The derivation of the parabolic PDE model follows as above, and here we obtain the following three component system:

$$(10) \quad \begin{aligned} \frac{\partial u}{\partial t} &= D_u \frac{\partial^2 u}{\partial x^2} - \frac{\partial}{\partial x} \left(\beta(w) u \chi(v) \frac{\partial v}{\partial x} \right) + f(u, v, w) \\ \frac{\partial v}{\partial t} &= D_v \frac{\partial^2 v}{\partial x^2} + g_1(u, v, w) \\ \frac{\partial w}{\partial t} &= D_w \frac{\partial^2 w}{\partial x^2} + g_2(u, v, w), \end{aligned}$$

where again, $\chi(v)$ is given by (5). In the special case where the quorum sensing molecule w is not diffusing and it is a monotone increasing function of the cell density, $w = w(u)$, we can replace $\beta(w) = \beta(w(u)) =: \phi(u)$. If we assume that w switches the response to v from attractant at low concentrations of w to repellent at high concentrations (e.g. $\beta(w) = 1 - w/w^*$), then the connection with the model of [19] becomes apparent and we may reasonably expect global existence in certain scenarios.

Here, the density to which cells fill-up is not necessarily the maximum volume, but to a level determined by the concentration of w .

3.3.2 Mediating at gradient detection A second possibility is that w interferes at the level of gradient sensing, in which case:

$$\mathcal{T}_n^\pm = \alpha + \beta (\tau(v_{i\pm 1}, w_{i\pm 1}) - \tau(v_i, w_i))$$

Assuming $\mathcal{T}_n^\pm \geq 0$ we substitute this into Equation (3) and derive the PDE:

$$\begin{aligned}
 \frac{\partial u}{\partial t} &= D_u \frac{\partial^2 u}{\partial x^2} - \frac{\partial}{\partial x} \left(u \chi_v(v, w) \frac{\partial v}{\partial x} \right) \\
 &\quad - \frac{\partial}{\partial x} \left(u \chi_w(v, w) \frac{\partial w}{\partial x} \right) + f(u, v, w) \\
 \frac{\partial v}{\partial t} &= D_v \frac{\partial^2 v}{\partial x^2} + g_1(u, v, w) \\
 \frac{\partial w}{\partial t} &= D_w \frac{\partial^2 w}{\partial x^2} + g_2(u, v, w)
 \end{aligned}
 \tag{11}$$

Thus, the migration of cells is dictated by gradients in both v and w . Dual-gradient systems have been considered in [44], where a number of possibilities for how multiple chemical signals are integrated at the level of the cell surface have been examined. For example, w may bind to the chemoattractant receptors, thereby reducing the availability of free receptors for v to bind to.

Again it is possible to make the connection with the model of [19] by considering special-case scenarios. For example, we may consider the following simple dual gradient system:

$$\begin{aligned}
 u_t &= D_u u_{xx} - \chi_v (uv_x)_x + \chi_w (uw_x)_x \\
 v_t &= D_v v_{xx} + u - v \\
 w_t &= D_w w_{xx} + \gamma uv - \delta w
 \end{aligned}
 \tag{12}$$

Here χ_v, χ_w are considered constant. In this model, the amount of secretion of w is regulated by the amount of chemoattractant detected by the cells. Under the assumption that γ and δ are large, and D_w is small we can make the first order approximation $w \sim \rho uv$, where $\rho = \gamma/\delta$. Substituting this into the equation for u gives

$$\begin{aligned}
 u_t &= ((D_u + \rho \chi_w uv) u_x)_x - (u (\chi_v - \chi_w \rho u) v_x)_x \\
 v_t &= D_v v_{xx} + u - v
 \end{aligned}$$

This is essentially the same form as Equations (1), however here the diffusion term is dependent on u and v . Since diffusion has a stabilising effect on gradients, we would expect similar behaviour for this system, and simulations later confirm this intuition.

In fact, the above may reasonably describe certain behaviours in *E.coli* and other bacteria; which are shown to demonstrate both attractant responses to substances such as food, and repellent responses from noxious or toxic substances. Aerobic respiration of *E. Coli* results in the generation of a number of toxic byproducts, such as hydrogen peroxide (e.g. [24]) and chemorepulsion to gradients of hydrogen peroxide have been demonstrated, e.g. [3],

3.4 Steady states for the volume filling model We can obtain a better understanding into the form of the steady states to the chemotactic model by analysing the problem in more detail. Here we exclusively consider the volume-filling model, Equations (8), without cell population dynamics. The cell density for this model evolves according to:

$$u_t = \left(D_u(q(u) - q'(u)u)u_x - \chi_0 q(u)u\tau_x \right)_x.$$

We study this equation on the interval $[0, l]$ with homogeneous non-flux boundary conditions:

$$(13) \quad D_u(q(u) - q'(u)u)u_x - \chi_0 q(u)u\tau_x = 0, \quad \text{at } x = 0, l.$$

For chemosensitive movement the parameter function τ is a function of the signal concentration $v(t, x)$, where v satisfies a parabolic Neumann problem (second equation of (1)). Thus, at the boundary:

$$\tau_x = \tau'v_x = 0, \quad \text{at } x = 0, l.$$

and consequently

$$(q(u) - q'(u)u)u_x = 0, \quad \text{at } x = 0, l.$$

Steady states satisfy $u_t = 0$. With the boundary conditions (13) it follows that on $[0, l]$

$$(14) \quad D_u(q(u) - q'(u)u)u_x = \chi_0 q(u)u\tau_x$$

We study several cases.

3.4.1 The function $\tau(x)$ is given For a given function $\tau(x)$ and the standard case of volume filling: $q(u) = 1 - u$, we have $q(u) - q'(u)u = 1$ and (14) leads to a logistic equation

$$(15) \quad u_x = \mu(x)u(1 - u), \quad \text{on } [0, l]$$

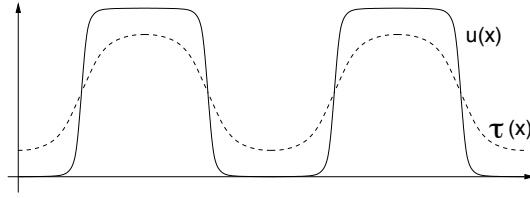


FIGURE 2: Example of a two-peak steady state solution for u .

with

$$(16) \quad \mu(x) := \frac{\chi_0}{D_u} \tau_x(x).$$

Hence the numerically observed patterns are plateaus of level 0 or 1, which are connected by solutions of the logistic equation (15). In the case of increasing τ we have an increasing sigmoide curve, and for decreasing τ a decreasing sigmoide curve. We solve the boundary value problem for the logistic equation (15) using the standard separation ansatz.

$$(17) \quad u(x) = \frac{c}{e^{-M(x)} + c}, \quad \text{with } M(x) = \frac{\chi_0}{D_u} \tau(x).$$

The constant c is specified using conservation of mass:

$$\int_0^l u(x) dx = \bar{U}_0 = \int_0^l u_0(x) dx.$$

The given function $\tau(x)$ appears explicitly in (17). The solution follows the shape of $\tau(x)$. We show a two-peak example in Figure 2.

For general $q(u)$, with the same $\mu(x)$ as above (16), we obtain:

$$(18) \quad u_x = \mu(x) \frac{q(u)u}{q(u) - q'(u)u}.$$

This equation is also separable and the solution is given implicitly of the form

$$(19) \quad \frac{u}{q(u)} = ce^{M(x)}, \quad \text{where again } M(x) = \frac{\chi_0}{D_u} \tau(x)$$

and c is specified by conservation of mass. We denote the left hand side by

$$\Phi(u) := \frac{u}{q(u)}.$$

If we consider $q(u)$ to be decreasing (this includes the standard volume filling model), then we find:

$$\Phi'(u) = \frac{q - q'u}{q^2} > 0.$$

Hence Φ is strictly increasing, invertible and Φ^{-1} is also strictly increasing. The solution of (18) is therefore given by:

$$(20) \quad u = \Phi^{-1}(ce^{M(x)})$$

and once again $u(x)$ has the same profile as $\tau(x)$. For the example $q(u) = 1 - u$ we find

$$\Phi^{-1}(z) = \frac{z}{1+z}.$$

3.4.2 Steady states of the full chemotaxis model Here we use the above observations to study the volume filling model (9) in the following form

$$\begin{aligned} u_t &= (D_u(q - q'u)u_x - qu\tau'(v)v_x)_x \\ v_t &= D_v v_{xx} + \gamma u - \delta v \end{aligned}$$

on $[0, l]$ with boundary conditions

$$(21) \quad v_x = 0, \quad \text{and } (q - q'u)u_x = 0$$

at $x = 0, l$.

A suitable non-dimensionalisation of variables x, t and v allows us to rewrite the above system as:

$$(22) \quad u_t = (D(q - q'u)u_x - \chi_0 qu\tau'(v)v_x)_x$$

$$(23) \quad v_t = v_{xx} + u - v$$

where D and χ_0 are constants and q, q', τ, τ' have been replaced with their non-dimensionalised counterparts. From the boundary conditions it follows that steady state solutions satisfy

$$(24) \quad D(q - q'u)u_x = \chi_0 qu\tau'(v)v_x$$

$$(25) \quad 0 = v_{xx} + u - v,$$

We solve equation (24) as above. Once more, u satisfies the logistic-type equation (18) and the solution is given as

$$(26) \quad u = \Phi^{-1} \left(ce^{M(v(x))} \right), \quad \text{where now } M(v(x)) = \frac{\chi_0}{D} \tau(v(x)),$$

where c is again specified through mass conservation. Finally, with the use of the second equation (25), we obtain the following nonlinear elliptic boundary value problem for v :

$$(27) \quad v_{xx} - v = -\Phi^{-1} \left(ce^{M(v)} \right), \quad v_x|_{0,l} = 0.$$

Problem (27) is a standard elliptic boundary value problem. We use phase-plane methods to analyse this system.

3.4.3 Phaseplane analysis First of all we summarise some facts concerning Φ^{-1} and $f(v) := v - \Phi^{-1}(ce^{M(v)})$. As mentioned earlier Φ^{-1} is strictly increasing. Since $M(v)$ is also increasing, the map $\Psi(v) := \Phi^{-1}(ce^{M(v)})$ is a strictly increasing function. Moreover it is of sigmoide type.

The function $\Phi(u) = u/q(u)$ has a pole at $u = 1$ and $\lim_{u \rightarrow 1^-} \Phi(u) = +\infty$. Consequently we have $\lim_{z \rightarrow +\infty} \Phi^{-1}(z) = 1$. Thus

$$\lim_{v \rightarrow \infty} \Psi(v) = \lim_{z \rightarrow \infty} \Phi^{-1}(z) = 1.$$

Moreover we find

$$\Psi(0) = \Phi^{-1}(ce^{M(0)}) > 0.$$

We obtain two generic cases. In the first case there is only one intersection of $v \mapsto v$ with $\Psi(v)$. and in a second case there are at least three intersection points. The case of two intersection points is non generic.

Case 1: There is a unique v_0 with

$$v_0 - \Psi(v_0) = f(v_0) = 0.$$

Then $f'(v_0) > 0$. Now we introduce $Z = v_x$ and we write the steady state equation (27) as a system

$$(28) \quad \begin{aligned} v_x &= Z \\ Z_x &= f(v). \end{aligned}$$

The linearization at $(v_0, 0)$ is

$$\begin{pmatrix} v \\ Z \end{pmatrix}' = \begin{pmatrix} 0 & 1 \\ f'(v_0) & 0 \end{pmatrix} \begin{pmatrix} v \\ Z \end{pmatrix}$$

The determinant of the corresponding Jacobian is $-f'(v_0) < 0$. Hence $(v_0, 0)$ is a saddle point with eigenvalues $\pm\sqrt{f'(v_0)}$ and eigenvectors

$$\begin{pmatrix} 1 \\ \pm\sqrt{f'(v_0)} \end{pmatrix}.$$

Due to Neumann boundary conditions we require $Z(0) = 0$ and $Z(l) = 0$. Except for the steady state $(v_0, 0)$ there is no trajectory which connects the v -axis with itself. This leads to the following:

Lemma 3.1. *If $v - \Psi(v)$ has only one zero v_0 then the unique steady state is the homogeneous distribution $(v(x), Z(x)) = (v_0, 0)$.*

Case 2: There are at least three zeros of single multiplicity $v_0 < v_1 < v_2$. Then we necessarily have $f'(v_0) > 0, f'(v_1) < 0, f'(v_2) > 0$. Hence $(v_0, 0)$ and $(v_2, 0)$ are both saddle points. The linearization at $(v_1, 0)$ gives a centre point. Let $F(v)$ denote a primitive of $f(v)$, then

$$H(v, Z) = F(v) - \frac{Z^2}{2}$$

defines an energy functional for system (28). Hence $(v_1, 0)$ indeed is a centre. The eigenvalues of the linearization around $(v_1, 0)$ are $\pm i\sqrt{|f'(v_1)|}$. Then solutions of (28) near $(v_1, 0)$ are composed of $\cos(\sqrt{|f'(v_1)|}x)$ and $\sin(\sqrt{|f'(v_1)|}x)$. The minimum interval length l^* that allows for a nontrivial connection from $Z(0) = 0$ to $Z(l^*) = 0$ is the length which corresponds to a half period of the above sin, cos functions. Hence

$$l^* = \frac{\pi}{\sqrt{|f'(v_1)|}}.$$

If l is sufficiently large then solutions are possible which loop around $(v_0, 0)$ more often. These correspond to multi-peak steady states.

3.5 Existence of solutions We will not go into details of proving existence and uniqueness of solutions to the aforementioned models. However, as this is an important issue we add some remarks on what we expect.

In comparison to the results of [19], Equation (1) has the additional term $f(u, v)$. This term does not involve derivatives, and is therefore of lower order than the diffusion or drift terms. Thus, if f is smooth enough we expect local existence of solutions in Sobolev spaces. Moreover, if solutions to the pure kinetic problem

$$u_t = f(u, v), \quad v_t = g(u, v)$$

exist globally in time, we may expect the same for the volume filling model (9). It has previously been shown, [4] that a strong decay in f for high particle densities u can control an aggregation force which, without f , would lead to finite time blow-up.

The existence of solutions for the quorum sensing models (10) and (11) is less straightforward. However, as we demonstrated above, certain scenarios lead to models very closely related to the system given by Equations (1), and it is therefore appropriate to assume that under reasonable choices of $\beta, f, g_1, g_2, \chi_v, \chi_w$ we expect no problems. The exact conditions needed for these parameters must be made precise elsewhere.

In the following sections we shall explore behaviour of the above systems by numerically solving the equations. In particular, we shall look at two phenomena commonly explored in mathematical modelling: travelling wave formation and pattern formation.

4 Propagation waves Travelling wave behaviour has been extensively studied in chemotactic systems, and applied to a variety of problems ranging from bacteria movement [27, 25, 39, 37], to angiogenesis in wound healing and tumour growth, [9, 40, 48]. In many studies of travelling wave behaviour, a key focus of attention is on how the wave-speed depends on the various system parameters [23]. In wound healing, for example, controlling the speed may have beneficial effects following surgery. We study the implications of the density dependence in the equations on the wave speed and compare with the wave speed in classical models of chemotactic growth.

4.1 Linear concentration gradient We consider a population of chemotactic cells in a constant chemoattractant gradient, $v_x = \text{constant}$, where the chemotactic sensitivity dependence on v is constant,

and the density dependence is given by $\phi(u)$. Coupling this with logistic cell kinetics gives:

$$(29) \quad \frac{\partial u}{\partial t} = D \frac{\partial^2 u}{\partial x^2} - \chi_0 \frac{\partial u \phi(u)}{\partial x} + ru(1-u).$$

This is effectively the classical Fisher wave equation with an additional convection term. We assume an infinite domain and initial conditions such that $u = 1$ for all $x \leq 0$ and $u = 0$ for $x > 0$. By converting to the travelling wave coordinate system $z = x - ct$ we derive an ODE for $U(z)$:

$$0 = DU'' + (c - \chi_0 (\phi + U\phi_u))U' + rU(1-U)$$

where $'$ denotes the derivative w.r.t. z , and $\phi_u = \frac{d\phi(u)}{du}$. By analysing the stability of steady states $(0, 0)$ and $(1, 0)$ in the phase plane:

$$(30) \quad \begin{aligned} U' &= V \\ V' &= -\frac{1}{D} \{ (c - \chi_0 (\phi(U) + U\phi_u(U)))V + rU(1-U) \}, \end{aligned}$$

it is straightforward to determine that $(1, 0)$ is linearly unstable, while $(0, 0)$ is stable with complex eigenvalues if $c < \chi_0\phi(0) + 2\sqrt{rD}$ and stable with real eigenvalues if $c \geq \chi_0\phi(0) + 2\sqrt{rD}$. Thus for solutions to remain relevant (i.e., ≥ 0), we must have:

$$c \geq c^* := \chi_0\phi(0) + 2\sqrt{rD}.$$

Indeed we find that c^* is the minimum wave speed:

Proposition 1. *For the classical case of $\phi(u) = 1$ and for the volume filling case of $\phi(u) = 1 - u$ there exists a travelling wave solution for equation (29) for each speed*

$$c \geq c^*.$$

Proof: For the case of $\phi(u) = 1$ we transform the speed as $\tilde{c} = c - \chi_0$. Then (30) with speed \tilde{c} has exactly the same form as for the corresponding Fisher equation without drift. Then the minimal wave speed is $\tilde{c}^* = 2\sqrt{rD}$ (e.g. [36]).

For the case of $\phi(u) = 1 - u$ we transform as $\hat{c} = (c - \chi_0)/\sqrt{rD}$ and apply a result of Murray and Gibbs (see [35]). There it is shown that $\hat{c}^* = 2$ is the minimum wave speed.

Simulations confirm that there is no difference in the wave speeds of the classical and the volume filling model.

4.2 Waves with cell growth and chemical kinetics We now assume that the chemical gradient is altered by the cell density according to the following model:

$$\begin{aligned}\frac{\partial u}{\partial t} &= D \frac{\partial^2 u}{\partial x^2} - \chi_0 \frac{\partial}{\partial x} \left(u \phi(u, v) \frac{\partial v}{\partial x} \right) + ruv \\ \frac{\partial v}{\partial t} &= \frac{\partial^2 v}{\partial x^2} - uv\end{aligned}$$

with initial conditions $v(x, 0) = 1.0$, and $u(x, 0)$ such that $u = u_s$ at $x = 0$ and $u = 0$ for $x > 0$. This models a simple experiment where a small population of bacteria is inoculated at the centre of a petri dish containing a suitable nutrient environment. Simulations indicate that following the initial stages of evolution, solutions settle into travelling wave behaviour, examples of which are shown in Figure 3(a). We compare the form and speed of waves generated under two choices of $\phi(u)$: (i) the classical model, $\phi(u) = 1$ and (ii) the volume-filling model, $\phi(u) = 1 - u$. At low values of χ_0 , there is no appreciable difference in solutions to the above equations, and wavespeeds are similar. However, as we increase χ_0 , travelling waves with the volume filling approach move more slowly compared to the corresponding waves using the classical approach, see Figure 3(b), and the wave has a much shallower form.

By putting a dependence in the sensitivity such that the nature of the molecule switches from attractant at low concentrations to repellent at higher densities (i.e., $\phi(u, v) = 1 - v$), we see a much different wave profile emerge. For sufficiently strong chemotaxis, a peak develops in the cell density at the front of the wave, Figure 3(c). Such rings have been observed in the swarming edges of bacterial colonies in petri dish experiments.

5 Pattern formation Pattern formation due to chemosensitive movement is seen in bacteria such as *E. coli* and *S. typhimurium*. *E. coli* have been shown to form a range of patterns, including rings and spots as they spread out in a nutrient environment [7, 8]. Chemotactic models similar to those proposed earlier have been demonstrated to explain these patterns, [64, 63, 62, 14]. In other applications chemotaxis equations have been applied to several processes of pattern formation in development, for example in the formation of pigmentation patterns, [45].

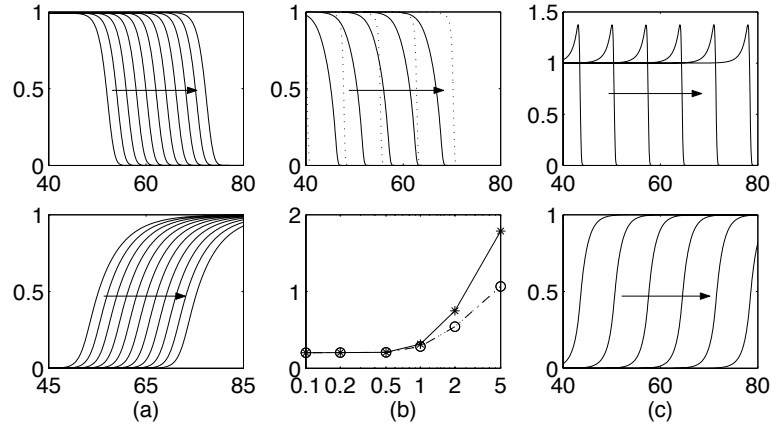


FIGURE 3: Column (a): Typical cell density (top) and chemical concentration travelling wave profiles for the model for low chemotactic strengths ($\chi_0 = 0.5$). Note that the results were very similar for all choices of chemotactic sensitivity, $\phi = 1$, $1 - u$, or $1 - v$. Wave direction indicated by arrows. (b) Top: Difference in wave profiles for the chemotactic sensitivity terms $\phi = 1$ (dotted) and $\phi = 1 - u$ (solid) for $\chi_0 = 2.0$. Bottom: Comparison of numerically calculated wave speed for different chemotactic strengths for $\phi(u) = 1$ (solid) and $\phi(u) = 1 - u$ (dashed). (c) For a chemotactic sensitivity term of the form $\phi = 1 - v$, a peak developed at the front of the cell density wave (top). Bottom graph shows the chemical concentration. For all simulations, other parameters are given by $r = 1.0$, $D = 0.01$, $u_s = 0.01$, with time steps of 10 between wave profiles

5.1 Linear analysis To understand the parameter regions where we may expect instability of a homogeneous solution, and thus the possibility of spatial patterning, a linear analysis can be performed (e.g., see [36]). The general model for chemotaxis with multiple chemotactic agents, including the models derived in Section 2 is given by the following equations:

$$u_t = \nabla \cdot \{D_u \nabla u - u \Phi(u, \mathbf{v}) \nabla \mathbf{v}\} + f(u, \mathbf{v})$$

$$\mathbf{v}_t = \mathbf{D}_v \nabla^2 \mathbf{v} + \mathbf{g}(u, \mathbf{v})$$

where u is the cell population, \mathbf{v} represents the n -vector of chemical species, Φ represents the n -vector of chemotactic sensitivities, \mathbf{D}_v is

the diagonal matrix of chemical diffusion rates and f and \mathbf{g} are cell and chemical kinetics. On a smooth domain Ω we assume zero-flux boundary conditions:

$$D_u \nabla u \cdot \eta - u \sum (\Phi_i(u, \mathbf{v}) \nabla v_i) \cdot \eta = 0$$

$$\nabla \mathbf{v} \cdot \eta = 0,$$

where η denotes the outer normal at $\partial\Omega$. We assume that the above system has a non-trivial steady state solution (u^*, \mathbf{v}^*) which is stable in the absence of spatial terms. We assume $D_u = \text{constant}$ and restrict attention to the one-dimensional domain $[0, L]$. We linearise the above system about the spatially homogeneous steady state (u^*, \mathbf{v}^*) . Solutions which satisfy the boundary conditions have the form $\cos(kx)e^{\lambda t}$, where λ is the eigenvalue determining temporal growth and k is commonly referred to as the wavenumber. The *dispersion relation* is derived by the following equation:

$$(31) \quad \begin{vmatrix} -D_u k^2 - \lambda + f_u & u^* \Phi(u^*, \mathbf{v}^*) k^2 + f_v \\ \mathbf{g}_u & -\mathbf{D}_v k^2 + \mathbf{g}_v - I\lambda \end{vmatrix} = 0$$

In the event that there exists a range of positive k^2 for which the eigenvalue λ has positive real parts, then perturbations to the homogeneous solution grow with time and the homogeneous solution is unstable. In such scenarios we may expect spatial patterning. Note that only discrete values of k will satisfy the boundary conditions, $k = \frac{n\pi}{L}$, where $n \in \mathbf{Z}$ is termed the *wavemode* and corresponds to the number of peaks such that $n = 2$ describes a 1 peak pattern, while $n = 3$ describes a $1\frac{1}{2}$ peak pattern.

We consider three cases:

Case 1: Zero cell kinetics, one chemical species

For $f = 0$ and a single chemical species, the characteristic polynomial determined from Equation (31) is:

$$0 = \lambda^2 + ((D_u + D_v) k^2 - g_v) \lambda + b_1(k^2)$$

$$b_1(k^2) = D_u D_v k^4 - (D_u g_v + g_u u^* \Phi(u^*, v^*)) k^2$$

where, by cell conservation, u^* is determined by the initial conditions. Since $g_v < 0$ (assuming stability of steady state in absence of spatial terms), instability of the uniform solution can only occur via $b_1(k^2) < 0$, hence necessarily

$$D_u g_v + g_u u^* \Phi(u^*, v^*) > 0$$

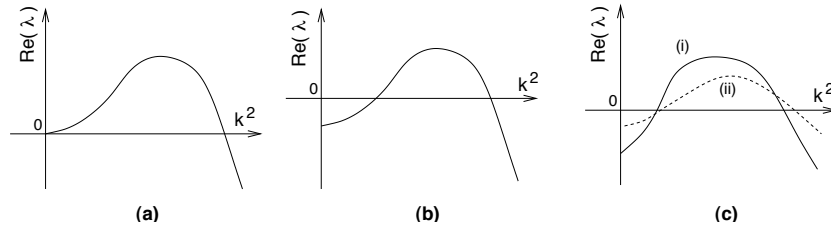


FIGURE 4: Typical dispersion relations where parameters predict an unstable range of wavenumbers for cases (1), (2) and (3). Solid lines refer to real eigenvalues, while dashed lines refer to complex eigenvalues

This provides conditions on the strength of chemotaxis for instabilities to occur. It is straightforward to see that the dispersion relation under this scenario leads to a range of k^2 given by $[0, k_u^2]$ for which $\text{Re}(\lambda) > 0$, Figure 4(a).

Case 2: Non-zero cell kinetics, one chemical species

For $f(u, v) \neq 0$ and a single chemical species, we can calculate the dispersion relation as:

$$\lambda^2 + ((D_u + D_v)k^2 - (f_u + g_v))\lambda + b(k^2) = 0$$

$$D_u D_v k^4 - (D_u g_v + D_v f_u + g_u u^* \Phi(u^*, v^*))k^2 + f_u g_v - f_v g_u = b_2(k^2)$$

Stability of the steady state for the corresponding kinetic equations (without diffusion) implies $f_u + g_v < 0$ and $f_u g_v - f_v g_u > 0$. Conditions for the steady state to be unstable here can be found, however now the range of unstable wavenumbers is given as $k^2 \in [k_l^2, k_u^2]$ where $k_l > 0$, Figure 4(b).

Case 3: Non-zero cell kinetics, two chemical species

With two chemicals, a cubic dispersion relation follows of the form:

$$0 = \lambda^3 + a(k^2)\lambda^2 + b(k^2)\lambda + c(k^2)$$

We note that stability of the steady state in the absence of spatial terms implies $a(k^2) > 0$ for all k . Stability can be lost either through $b(k^2) < 0$ or $c(k^2) < 0$. Note that several classes of dispersion relation can be found; shown are (i) a range of unstable wavenumbers with real eigenvalue and (ii) a range of unstable wavenumbers with complex eigenvalues. More complicated classes can also be found, for example those which show two non-connected ranges of unstable wavenumbers, which may have either real or complex eigenvalues. The type of instability must be studied separately in each application.

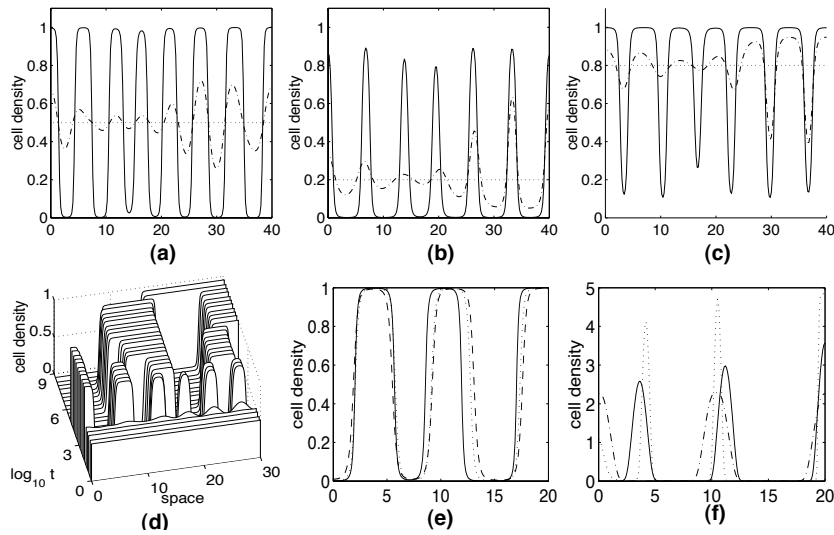


FIGURE 5: (a) Early evolution of a multi-peak pattern for Model (1) with $\chi(u, v) = \chi_0(1 - u)$ and with initial cell density of 0.5 shown at $T=0$ (dot), 20 (dot-dash) and 100 (solid). (b) Initial density = 0.2, at $T=0$ (dot), 50 (dot-dash) and 100 (solid). (c) Initial density = 0.8, at $T=0$ (dot), 50 (dot-dash) and 100 (solid). (d) Long time evolution for initial cell density of 0.5 showing coarsening to a single half-peak pattern. (e) $q(u) = 1 - u^\gamma$ for $\gamma = 4.0$ (solid), 1.0 (dot) and 0.25 (dash). We use a domain of length 20 and parameters $D_u = 0.25$ and $\chi_0 = 4.0$ Data is plotted at $T = 500$. (f) $q(u) = \exp(-\gamma u)$ for $\gamma = 1.0$ (dot, $T = 300.0$), 3.0 (dot-dash, $T = 5000$) and 5.0 (solid, $T = 5000$).

5.2 Pattern formation: simulations in one-dimension

5.2.1 *Zero Cell Kinetics* We consider the volume-filling chemotaxis system, given by Model (1) with cell kinetics $f(u, v) = 0$ and $\chi(u, v) = \chi_0(1 - u)$, $\chi_0 > 0$ a constant. Unless stated otherwise, throughout the following sections we shall assume chemical kinetics take the form $g(u, v) = u - v$, and zero flux boundary conditions. Initial conditions will be set at the homogeneous steady states, but spatially perturbing the chemical concentration by a small random amount.

For initial conditions $u(x, 0) = u_s$ (constant) the homogeneous steady state is $(u^*, v^*) = (u_s, v_s)$. The results of the linear stability analysis

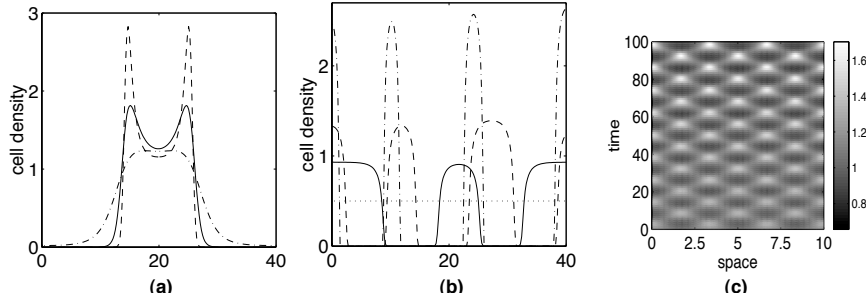


FIGURE 6: (a) Chemotaxis modulated by a secondary (quorum sensing) molecule, shown at $t = 2000$ for: $\chi_0 = 1.0$ (dot-dash line), $\chi_0 = 3.0$ (solid), $\chi = 10.0$ (dashed). Other parameters: $D_u = 0.1, D_w = 1.0, \delta = 1.0$ and an initial density of $u = 0.5$. (b) Density regulation in the attraction-repulsion system. Density profile at $t = 10000$ for chemorepulsion strength: $\chi_w = -1.0$ (dotted line), -0.75 (solid line), -0.5 (dashed), and -0.25 (dot-dash). Other parameters: $D_u = 0.02, D_v = 1.0, D_w = 0.1, \chi_u = 1.0, \delta = \gamma = 1$ on the domain of length 40. (c) Example of oscillating solutions in the three species attractant-repellent system.

indicate that we have instability of the homogeneous solution when

$$\chi_0 > \frac{D}{u_s(1 - u_s)}.$$

Under this scenario, from Figure 4(a) we expect all low wavemodes to be unstable. The cell density is crucial on the ability to form patterns: at low and high values of u_s , the system is stable to spatial perturbations. Effectively, this indicates that the chemoattractant with the above kinetics behaves as quorum-sensing molecule — there is a switch in the behaviour of the system from homogeneity (e.g. “vegetative swarming of bacteria”) to spatial patterning (i.e., “aggregation of bacteria”) through a change in the density of the population, mediated by the cell secreted chemoattractant molecule.

The above case was explored in [19]. Typical numerical simulations are shown in Figure 5(a–c) for a range of different initial cell densities. As expected from the above condition, for u_s close to 0 or 1, we do not get spatial patterning. In the region of instability a series of cell density peaks form. The growth at the peak is capped by the space filling mechanism, resulting in the formation of “density plateaus”. This is in

sharp opposition to those patterns generated by the classical chemotaxis model, where sharp spikes form in cell density. By varying the initial density of the cell population (shown in Figure 5(a)–(c) for $u_s = 0.5$, 0.2 and 0.8 resp.), the variation in the thickness and inter-width of these plateaus can be controlled. Thus the above mechanism forms a robust method of generating variations in cell density of varying thickness.

Subsequent evolution of the solutions results in a sequence of coarsening as peaks slowly merge and/or collapse. When ran for enough time, this results in a single half peak at the boundary, 5(d). This process can also occur for other chemotactic sensitivity forms, and bears similarities with coarsening processes described in Cahn-Hilliard models [60]. An intuitive understanding for the coarsening process in a related model for cell movement can be found in [43, 22]. The development of these patterns, the process of merging and coarsening and the appearance of ultra-long transients is studied in [50]. Simulations for different choices of space-occupancy function, $q(u)$ in Equation (9) are shown in Figure 5(e) and (f). In (e) we consider $q(u) = 1 - u^\gamma$ for $\gamma = 4, 1.0$ and 0.25 . Note that there is very little effect of γ on the form of the solutions. In (f) we choose $q(u) = \exp(-\gamma u)$. The absence of a u^* such that $q(u^*) = 0$ means that we can no longer apply the results of [19]. Higher choices of γ do limit the growth of an aggregate, yet low γ result in very sharp cell density aggregates.

We now consider the quorum/chemical-mediated approaches to incorporating density. From the linear analysis for a one-cell, two chemical system, we obtain a cubic dispersion relation, and correspondingly a much richer variety in solution behaviour, *cf* Figure 4(c).

Simulations of the model given by Equations (10) are shown in Figure 6(a), for the same chemical dynamics as above for v , and $\chi(v) = \chi_0$, $\beta(w) = (1 - w)$ and $g_2(u, v, w) = u - \delta w$. Here the mechanical response of cells to the chemical v is either attractant or repellent, depending on the local concentration of a secondary molecule, w . Once again, this mechanism provides an effective method of controlling population density in aggregations. However, as we alter the strength of the chemotactic term, the shape of the aggregation changes from a simple aggregation to a “split-peak” pattern, with the cell density higher at the edge of the aggregation. This pattern emerges as a result of the high levels of w in the centre of the aggregation switching the behaviour to chemorepulsion.

The “attractant-repellent” system, Equations (11), also provides a mechanism for density control, as we indicate by the simulations in Figure 6(b) using model equations (12). Here, by altering the strength of the chemorepulsion, we can switch from high density aggregations to low

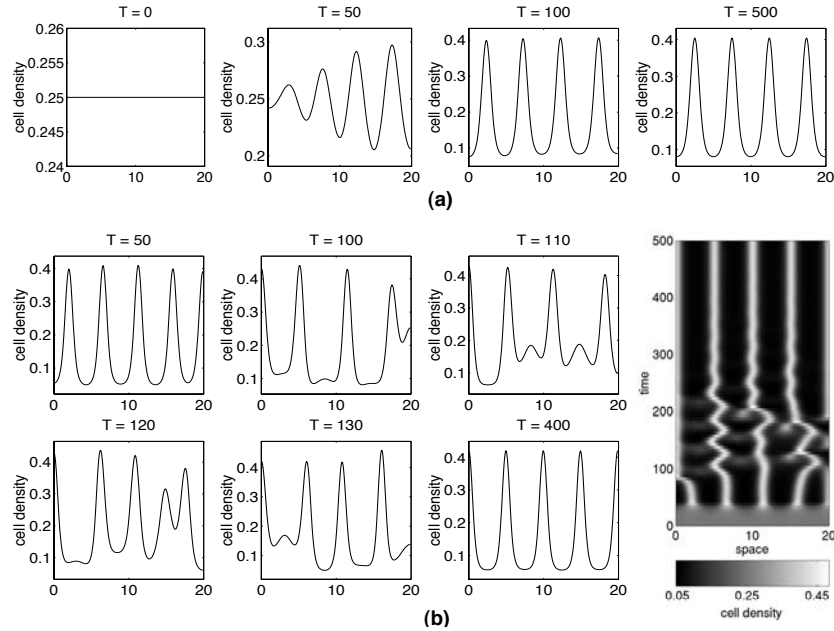


FIGURE 7: (a) Time sequence showing cell density evolution for simulation of Equations 1 with cell kinetics $f(u, v) = ru(1 - u/u_m)$. Here, parameters $r = 0.5$, $u_m = 0.25$, $\chi_0 = 9$, $D = 0.25$ define a point close to the stability/instability boundary, and we solve on $[0, 20]$ with zero-flux boundary conditions. (b) Time sequence showing cell density for parameter set $r = 0.5$, $u_m = 0.25$, $\chi_0 = 10$, $D = 0.25$ on the domain $[0, 20]$. During early evolution, solutions demonstrate temporal dynamics before stabilising into the pattern shown at $T = 400$. The full sequence is illustrated by the space-time plot on the right showing cell density evolution.

density aggregations. The additional solution classes predicted by the linear analysis can be derived under suitably chosen kinetics/parameters. When kinetics and parameters were chosen such that a dispersion relation of the form Figure 4(c), (ii) (i.e., complex eigenvalues) was obtained, the solutions oscillate both spatially and temporally, Figure 6(c).

5.2.2 Inclusion of cell kinetics The no-cell kinetics scenario demonstrates aggregation. However the evolution demonstrated a coarsening process during which the wavelength of the pattern increased until a

single large aggregation is left. In many developmental processes of aggregation, the number and/or size of aggregations is carefully controlled: for example in the fruiting-body aggregations seen in *Myxobacteria* or *Dictyostelium*, the number of cells is carefully controlled to provide optimum conditions for subsequent spore dispersal.

Of course, the zero-cell kinetics model does admit multiple aggregations, which can exist over large time scales (cf. Figure 5(d)). However, whether this is “robust enough” for processes of development is clearly an issue. To explore whether stable multi-peak aggregation patterns can develop within the modified model, we incorporate the effect of cell kinetics into the model.

Type I: $f(u, v) = ru(1 - u/u_m)$

For the above logistic-type kinetics, the (non-trivial) homogeneous solution of (9) is given by: $(u^*, v^*) = (u_m, v_m)$, and instability of this steady state is determined by the following condition on the parameter values:

$$0 < 2\sqrt{Dr} < u_m(1 - u_m)\chi_0 - (r + D)$$

From our linear stability analysis, our dispersion relation now corresponds to Figure 4(b). Thus, low wavemodes may now be stable to spatial perturbation, and we can expect that, at least initially, higher wavemodes corresponding to multi-peak solutions may develop.

We choose a set of parameter values such that we are just within the instability region, and plot the results in Figure 7, sequence (a). Time-evolution shows that multiple-peaked solutions develop, and simulations indicate that they exist indefinitely. For u_m well below 1, the volume filling effect has little difference, and solutions are very similar to those resulting from the classical chemotactic model.

Applied to physical problems, it is crucial to understand how the solution behaviour varies deeper in the instability region, since the precision to which parameters can be controlled is debatable. A typical simulation is shown in sequence Figure 7(b). Although the pattern eventually settles into a fixed pattern ($T = 400$ plot), the initial evolution shows a temporally oscillating pattern as some peaks collapse together (e.g. see frames $T = 100 - 130$). The space time plot showing how the cell density evolves is indicated in the right hand plot.

This behaviour is even more pronounced further into the instability region, as indicated by the space-time plots Figure 8(a)–(c). Simulations indicate that a time-independent spatial pattern does not form, and solutions remain locked in a continuous process of “merging and

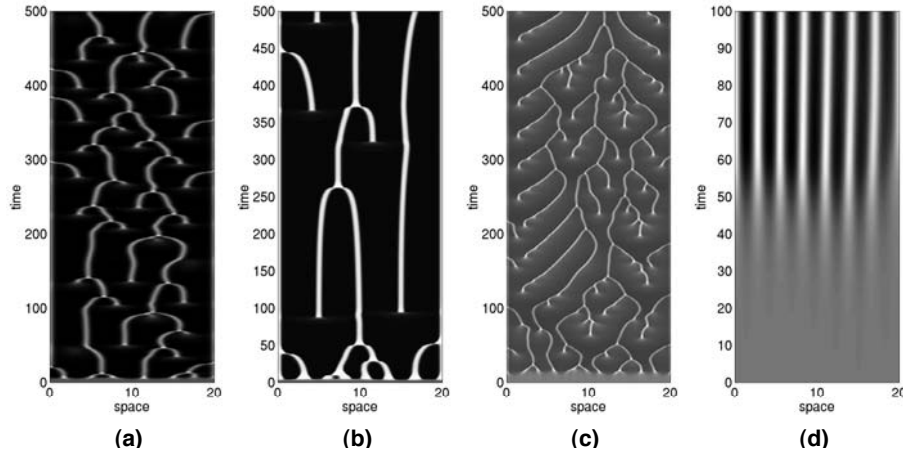


FIGURE 8: Space-time plots for evolution of cell density in different regions of parameter space. (a) $r = 0.5, u_m = 0.25, \chi_0 = 20, D = 0.25$: Numerics indicate that a fixed spatial pattern does not occur, as new peaks constantly emerge and merge. (b) $r = 0.5, u_m = 0.75, \chi_0 = 20.0, D = 0.25$. (c) $r = 0.25, u_m = 0.25, \chi_0 = 5.0, D = 0.01$. (d) Closer to the stability/instability boundary a stable pattern emerges, here the 7 peak solution $r = 0.25, u_m = 0.25, \chi_0 = 2.0, D = 0.01$. All simulations use the domain size $[0, 20]$.

emerging”. Cell aggregations join together to form a single aggregation, resulting in a large space of low cell density. In the low density regions, new cell aggregations subsequently arise. Examples at a variety of points deep within the instability region are shown in Figure 8(a)–(c), and the contrast with a point close to the stability-instability boundary is indicated by Figure 8(d), where a time-independent 7-peak pattern evolves.

Type II: $f(u, v) = ruv(1 - u/u_m)$

An alternative choice of cell kinetics can lead to stable aggregations, even well within the instability region. For the above, we assume that the chemical mediates both cell migration and cell proliferation. In fact, many growth factors have been shown to stimulate such dual activity: for example, VEGF mediates both endothelial cell proliferation and chemotaxis. Using the above kinetics, solutions demonstrate the same initial period of coarsening seen in earlier models, however aggregations eventually settle into a time-independent multi-peak structure. Here

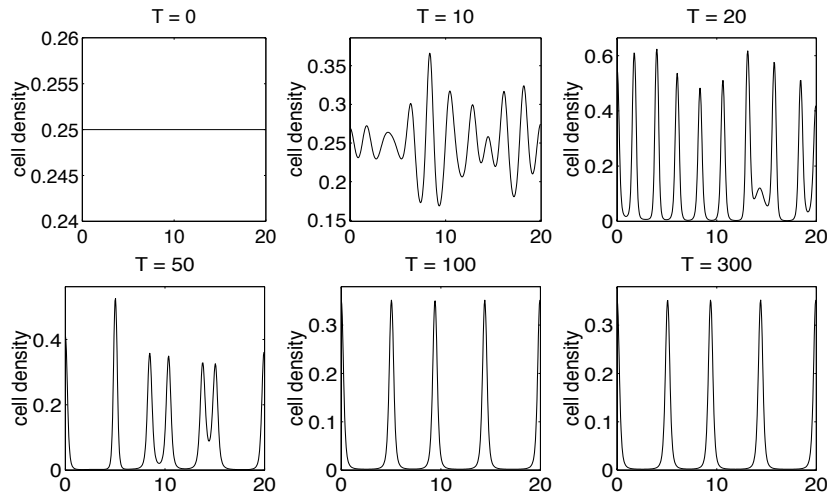


FIGURE 9: Snapshots for a typical evolution for kinetics given by $f(u, v) = ruv(1 - u/u_m)$. Here, $r = 0.5$, $u_m = 0.25$, $\chi_0 = 10.0$, $d = 0.25$ and the domain is $[0, 40]$ (here 401 grid points used).

the dependency on the chemical limits new proliferation at the troughs, and thus new peaks do not emerge. A typical example is shown in the sequence of Figure 9.

5.3 Two-dimensional simulations

5.3.1 Zero cell kinetics We extend our numerical investigation to two dimensions. Here, the difference between the behaviour in the classical chemotactic system and the density regulated model become more apparent. For the classical chemotactic systems, where the chemotactic velocity depends linearly on the cell density, several studies have shown that blow-up occurs.

The volume filling mechanism excludes such behaviour. Instead, when (9) with $q(u) = 1 - u$ is solved on a two-dimensional domain, the pattern that initially develops undergoes the same process of coarsening observed in the one-dimensional case, Figure 10, top row. We expect that the coarsening procedure, if ran for sufficient time, will eventually result in the cells accumulated into a single aggregation. For an initial density of $u_s = 0.5$, the type of pattern that develops has a labyrinthian structure, however by changing this value we can see a transition to spots (at lower

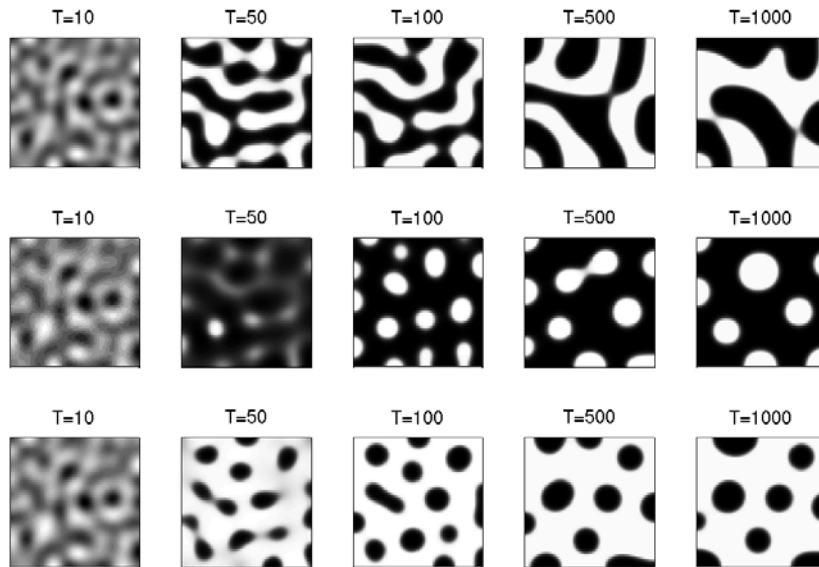


FIGURE 10: Coarsening process in the two-dimensional model with no cell kinetics. Top row $u(x, y, 0) = 0.5$, Middle row: $u(x, y, 0) = 0.25$, Bottom row: $u(x, y, 0) = 0.75$. Colourscale shows cell density (black = low cell density, white = high cell density). Parameters are $D_u = 0.25, \chi = 4.0$ on the domain $[0, 25] \times [0, 25]$.

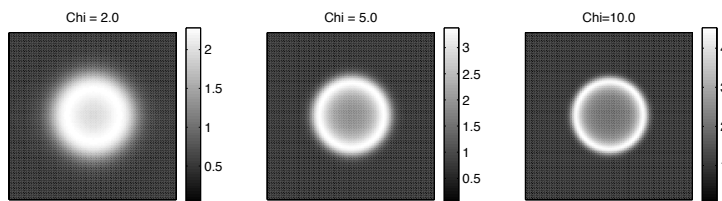


FIGURE 11: Two dimensional patterns generated using the quorum/chemical mediated approaches of Section 2. Here, depending on the system parameters, we can see the formation of ring structures.

initial densities, Figure 10 middle row) or inverted spots/honeycomb patterns (at higher initial densities, Figure 10 bottom row). This transition of patterns is reminiscent of those observed both experimentally ([42]) and numerically ([32, 38]) in Turing systems ([61]). It has been found analytically that the formation of stripes or spots depends strongly upon the nonlinearities in the kinetic terms, [15, 31]).

The chemical mediated models also provide mechanisms to limit the population, as the results in one-dimension would lead us to expect. We show typical numerical simulations for the model given by Equations (10) in Figure (11). The “split-peak” patterns seen in one dimension translate to ring patterns in two dimensions.

5.3.2 Nonzero cell kinetics Incorporating cell-kinetics of the form $ru(1 - u/u^*)$ into (9) resulted in merging-emerging process in one dimension. This is also seen in two dimensions, as demonstrated by the time sequence shown in the sequence Figure 12(a). Shifting one of the parameters (here we choose r) closer to the border between instability/stability of the steady state, we move from a pattern of spots to a more labyrinthian structure, or strands. The merging-emerging process continues to take place, as shown by Sequence 12(b), however after a while the stripes become orientated with respect to the boundaries. Moving even closer to the stability/instability boundary stable patterns can form, as our results in one dimension indicated. Shown in Figure 12(c) is a honeycomb lattice pattern. The above sequence of pattern types as a parameter is varied was found to be typical of those seen in other parts of the parameter space. Cell kinetics of the form $f(u, v) = ruv(1 - u/u^*)$ resulted in a pattern of multiple stable cell aggregations (spots).

6 Pattern formation on growing domains Embryonic development requires extensive tissue growth and deformation. Models for patterning applied to such processes must therefore consider the potential implications of domain growth.

In previous studies, a large amount of attention has focussed on the patterning resulting from solving Turing-type systems on growing domains, [2, 28, 45, 11]. When solved on a growing one-dimensional domain, new peaks in the chemical pattern are inserted as the domain grows in a manner such that the inherent wavelength of the pattern is (roughly) conserved. This was applied by Kondo and Asai to the particular problem of pigmentation patterns seen on species of marine angelfish.

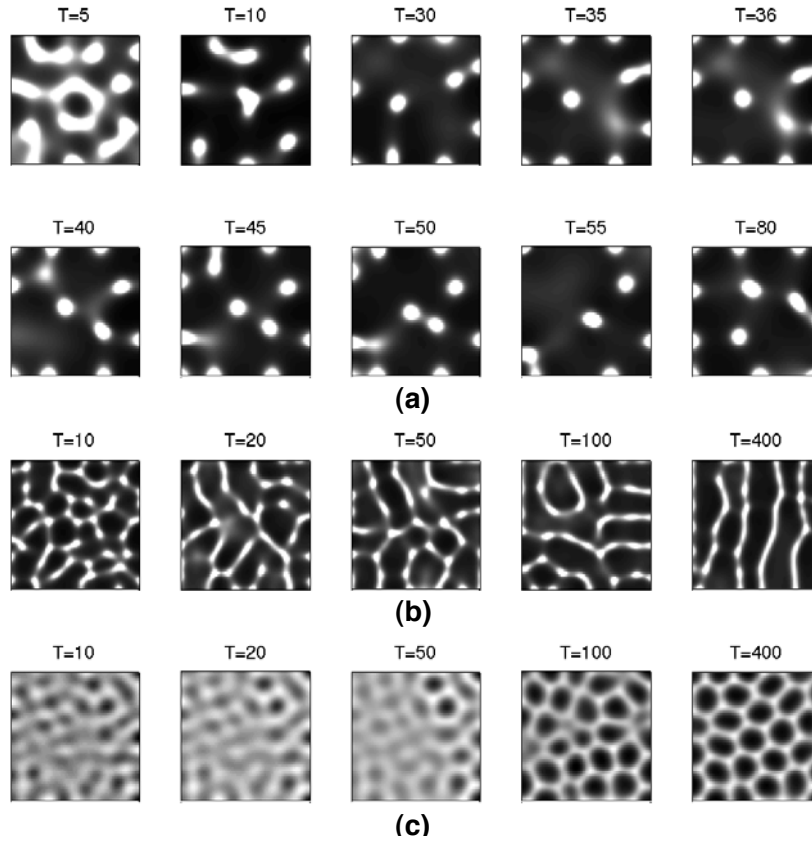


FIGURE 12: Patterning in the two-dimensional cell kinetics model. (a) Time evolution of cell density for $r = 0.5$ on the domain 10×10 . Black-White gray-scale indicates density from 0.0 to 0.3. (b) Time evolution of cell density for $r = 1.0$ on the domain 20×20 . Black-White gray-scale indicates density from 0.0 to 0.4. (c) Time evolution of cell density for $r = 2.0$ on the domain 20×20 . For all simulations, we set other parameters at $D_u = 0.25$, $u_{\max} = 0.25$, $\chi = 20$ with (step size = 0.001, 101×101 grid points).

Juvenile members of *Pomacanthus* display prominent pigment stripes on the body. As the fish grows and doubles in length, new pigment stripes are inserted between the existing stripes. The model of Kondo and Asai was augmented in [45] to incorporate chemotactic movement by the pigment cells to show additional features of the patterning phenomena.

Many patterning processes in development, however, require that the structure of the pattern remains the same, despite any subsequent tissue growth — For example, we only have two lungs, or one heart. Again, examples can be found in fish pigmentation patterns; many species of fish (e.g. members of the butterfly fish, *Chaetodon*) display a single prominent spot on the flank. This often serves function as a “false eye”, confusing potential aggressors into attacking less vulnerable parts. In many other examples, the pigmentation pattern simply expands as the fish grows.

We investigate the behaviour of the volume-filling chemotaxis model (1) on a domain $[0, L]$, growing exponentially such that $L(t) = L_0 \exp(rt)$. A rescaling of space transforms the chemotaxis system on a growing domain onto a time-independent domain, $[0, L_c]$, where L_c is constant and:

$$\begin{aligned} \frac{\partial u}{\partial t} &= \exp(-2rt) \frac{\partial}{\partial x} \left\{ D_u \frac{\partial u}{\partial x} - \chi_0 u(1-u) \frac{\partial v}{\partial x} \right\} + f(u, v) - ru \\ \frac{\partial v}{\partial t} &= D_v \exp(-2rt) \frac{\partial^2 v}{\partial x^2} + g(u, v) - rv \end{aligned}$$

See [45] for further details of the derivation. Thus, the diffusion/chemotactic coefficients are now time-dependent. The $-ru, -rv$ terms can be thought of as a dilation effect: as the domain grows, the existing cells/chemical must be “stretched” over a larger region.

6.1 Patterning under different growth rates In Figure 13(a)–(c) we show space-time plots of the cell density for different choices of growth rate r . Note that we have re-scaled space to represent the actual domain size. For cell kinetics we have assumed that the cells grow at the same rate as the domain expands; thus the growth function $f(u, v)$ cancels the dilation effect in the above equations. We choose the same chemical kinetics as before and simply absorb the chemical dilation into the decay term, i.e., $g(u, v) - rv = u - v$.

For a zero growth rate, we observe the coarsening process as previously described for the zero kinetics model, Figure 13(a). When growth is incorporated into the model ($r = 0.001$, Figure 13(b)), however, the coarsening process does not occur and the initial pattern selected (here,

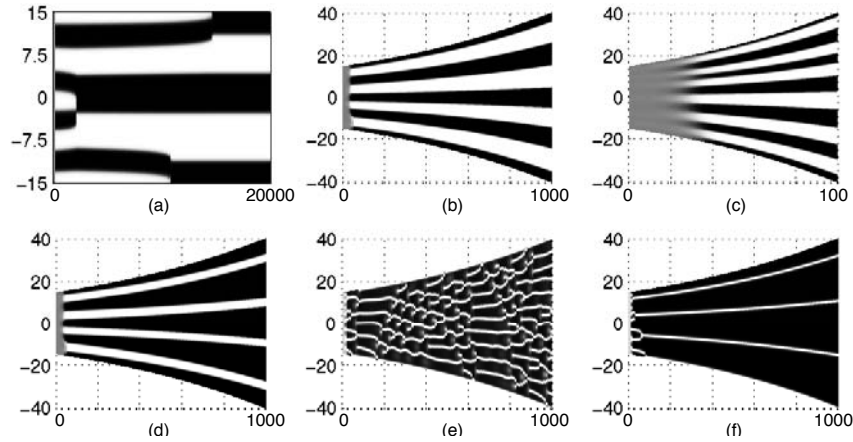


FIGURE 13: Evolution of the cell-chemotaxis model on a growing domain, $[0, L]$, where domain growth is given by $L(t) = L_0 \exp(rt)$. Space-time plots show the cell density where black represents low and white represents high density. In (a)-(c) we choose $f(u, v) = ru$, where (a) $r = 0$, (b) $r = 0.001$ (c) $r = 0.01$. Other parameters are $D_u = 0.25, D_v = 1.0, \chi_0 = 4.0$ and an initial domain of length 30. (d) $f(u, v) = 0$, other parameters as above (e) $f(u, v) = \gamma u(1 - u/u_m)$ with $u_m = 0.25, \gamma = 0.25, D_u = 0.25, D_v = 1.0, \chi_0 = 10.0$ (f) $f(u, v) = \gamma uv(1 - u/u_m)$ with $u_m = 0.25, \gamma = 0.25, D_u = 0.25, D_v = 1.0, \chi_0 = 10.0$.

a 4 peak pattern), is preserved throughout subsequent domain growth. This general behaviour was found to preserve both at higher growth rates (e.g. $r = 0.01$, Figure 13(c)) and lower growth rates (not shown). However, at higher growth rates, the initial pattern selected had a shorter wavelength (in (c), a 6 peak pattern). This is likely a result of early solution behaviour.

These simulations indicate that the chemotaxis model is able to robustly generate a pattern that is insensitive to subsequent domain growth and expansion, thus distinct from the type of patterns created by Turing models on a growing domain. Clearly the chemotaxis model may be suitable to systems where the patterning is insensitive to domain expansion. Two dimensional simulations show the equivalent behaviour, Figure 14.

6.2 Other cell kinetics We consider the effects of different cell kinetics in the domain growth problem. In Figure 13(d), we choose zero cell

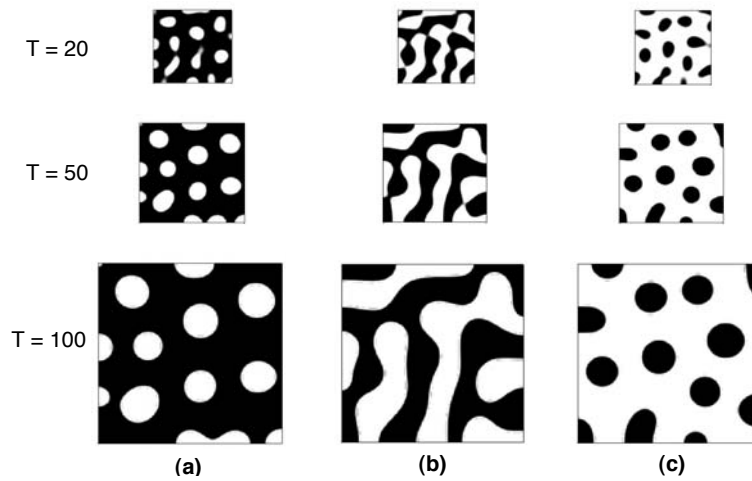


FIGURE 14: Evolution of the cell-chemotaxis model on a growing two-dimensional domain showing the preservation of (a) spot ($u_0 = 0.25$), (b) labyrinthian/stripe, ($u_0 = 0.5$), and (c) inverted spots ($u_0 = 0.75$).

growth (i.e., $f(u, v) = 0$). The cellular aggregations resulting in this scenario preserve the initial size of the aggregation throughout subsequent domain growth (as indicated by the width of the white region). This distinguishes the behaviour from the case where cell and domain growth correlate (i.e., Figure 13(b)), and the size of the cell aggregations grow.

In Figures 13(e) and (f) we choose the Type I and Type II kinetics discussed in the section for no domain growth. For Type I growth, we observe the complex “merging-emerging” pattern seen previously. Here, however, the average number of peaks increases as the domain gets larger. For Type II kinetics, the same pattern preservation behaviour as described above is observed.

7 Discussion Chemotactic movement is a widely employed mechanism for guidance at a multitude of scales. In this paper, we have derived a model of chemotaxis incorporating a density dependence in the chemotactic sensitivity function. This model was previously introduced in [19], where it was shown that under relevant chemical dynamics, solutions existed globally in time in all dimensions. Here we have demonstrated in depth how such models can naturally arise via incorporating appropriate biological details, including the space available for cells to migrate and

the response of cells to quorum-sensing molecules.

Modelling cell movement in dense environments has received scant attention to date. While detailed modelling requires close attention to the mechanics of interaction between individual cells, or between cells and the extracellular matrix; there is a strong need to develop models that phenomenologically capture the correct characteristics of the system, but remain amenable to both numerical and analytical insight. Here, we demonstrated how setting a threshold on cell occupancy at a position can lead to biologically realistic behaviour.

The dual role of chemicals as both attractants and repellents has been identified in many systems. In the developing nerve systems, growing nerve growth cones have been shown to be both attracted and repelled by a specific chemical, depending on the local environment [59, 58, 34], and similar responses have been identified in migrating mesoderm cells, [29] and immune cells [51]. Such dual responses are also found in bacteria; glycerol is both an attractant and repellent to *E. coli*, [66], while oxygen behaves both as an attractant and repellent for *S. typhimurium* and *E. coli*, depending on its concentration. The switching in the nature of a molecule from attractant to repellent can be employed as a mechanism for controlling population size when mediated by a quorum sensing molecule, as we demonstrate with the model, (10). “Quorum-sensing” has been shown to mediate a wide-range of behaviours in bacteria, including chemical synthesis and movement response. In our model, we showed how the regulation of the chemotactic movement via quorum-sensing type mediators provides a simple way of regulating the density of the aggregate. This can be employed in a multitude of ways; for example by switching the nature of a specific chemoattractant as above, or by finely tuned balancing of a combination of attractant and repellent cues. In the latter, we demonstrated how a simple model may give rise to careful control of group density. In fact, the model employed (Equations 12) could be interpreted as a highly simplified model for aerobic respiration of *E. coli*. *E. coli* are chemotactically attracted by oxygen gradients (aerotaxis) [53] however, aerobic respiration results in the generation of a number of harmful byproducts, such as hydrogen peroxide. The subsequent chemorepulsion away from the hydrogen peroxide (see [3]) would thus be necessary to limit the group size to a level at which the amount of hydrogen peroxide produced does not result in significant toxic damage.

The type of kinetics was shown to have a strong bearing on the type of patterning observed. Here we considered just three general forms. Choosing zero cell kinetics gives rise to a coarsening process during which

the wavelength of the pattern slowly increases. These dynamics may provide a robust mechanism for generating “unique” aggregation patterns; though clearly the timescales over which they can be generated remains an issue to be resolved (see [50]). Other kinetics gave rise to a perpetually evolving solution of “merging and emerging”. In these patterns, the average number of cell density peaks remained (crudely) consistent, however the spatial localisation of the peaks was continuously changing. Interestingly, in a few simulations, a stable (time-independent) pattern did sometimes emerge, indicating that such patterns can be stable. Clearly, understanding the stability of solutions for this system is an avenue for exploration. Intriguingly, many species of cacti (in particular, members of the *Cereus* family) display body patterns with a similar structure to the space-time plots shown in Figure 8. Although, the mechanism involved in the formation of these patterns is highly unlikely to involve cell movement, the striking similarity of the patterns is of interest.

A simple modulation of the kinetics, such that the cell proliferation was additionally dependent on the chemoattractant, gave rise to stable spatial patterns, and no emerging-merging behaviour was observed. Interestingly, many growth factors shown to induce motility have also been shown to have a mitogenic effect, and our results here suggests that such dual behaviour may have important consequences on the robustness of the patterns that emerge.

The question of pattern robustness is a crucial issue in development, in particular in scenarios where domain growth occurs. The incorporation of domain growth into Turing mechanisms has previously been shown to result in the alteration of the pattern such that more peaks are accommodated as the domain grows in size. While this may be appropriate in applications where the pattern changes with scale (e.g. certain fish pigmentation patterns) it is less desirable in other patterning processes. The simple chemotactic model presented here demonstrates how scale invariant patterns can be generated. Different choices of cell growth kinetics lead to patterns where the aggregation remains constant or grows as the underlying domain grows in size.

Several potential applications of the work here can be considered. For example, the early development of the vasculature arises as a result of two general processes. *Angiogenesis* is the sprouting of new capillaries from existing vasculature. *Vasculogenesis*, on the other hand, involves the spontaneous formation of new capillary networks from angioblast cells (endothelial cell precursors) in the mesoderm, see [17]. A number of basic growth factors have been demonstrated to play a role in

vasculogenesis; fibroblast growth factor 2 (FGF-2) induces the formation of the angioblast cells (endothelial cell precursors), while VEGF has been shown to play a critical role in the growth and development of the initial vascular pattern, [49]. VEGF has been shown to stimulate both proliferation of endothelial cells and chemotactic migration. As we demonstrated in Figure 12(c), a simple chemotactic model can give rise to a network like structure. Embryonic vasculogenesis, however, involves many other processes and regulatory growth factors, and clearly a detailed model exploring the generation of these patterns should be attempted elsewhere.

Acknowledgements The authors would like to thank Yasmin Dolak for thoughtful comments on the manuscript. KJP has been supported by SHEFC research grant 107. TH has been supported by NSERC research grant G121210825.

REFERENCES

1. B. Alberts, D. Bray, J. Lewis, M. Raff, K. Roberts, and J. D. Watson, *Molecular Biology of the Cell*, Garland Publishing Inc., New York, London, 1994.
2. P. Arcuri and J. D. Murray, *Pattern sensitivity to boundary and initial conditions in reaction-diffusion models*, *J. Math. Biol.*, **24** (1986), 141–165.
3. L. Benov and I. Fridovich, *Escherichia coli exhibits negative chemotaxis in gradients of hydrogen peroxide, hypochlorite, and n-chlorotaurine: products of the respiratory burst of phagocytic cells*, *Proc. Natl. Acad. Sci. USA*, **10**(93) (1996), 4999–5002.
4. A. Boy-Dalverny and M. Madaune-Tort, *Global solutions in three dimensions for systems describing chemotaxis phenomena*, *Adv. Appl. Math.*, **26**(1) (2001), 63–88.
5. D. A. Brock and R. H. Gomer, *A cell-counting factor regulating structure size in Dictyostelium*, *Genes. Dev.*, **13**(15) (1999), 1960–1969.
6. D. A. Brock, R. D. Hatton, D. V. Giurgiutiu, B. Scott, R. Ammann, and R. H. Gomer, *The different components of a multisubunit cell number-counting factor have both unique and overlapping functions*, *Development*, **129**(15) (2002), 3657–3668.
7. E. O. Budrene and H. C. Berg, *Complex patterns formed by motile cells of Escherichia coli*, *Nature*, **349**(6310) (1991), 630–633.
8. E. O. Budrene and H. C. Berg, *Dynamics of formation of symmetrical patterns by chemotactic bacteria*, *Nature*, **376**(6535) (1995), 49–53.
9. H. M. Byrne and M. A. J. Chaplain, *Mathematical models for tumour angiogenesis-numerical simulations and nonlinear-wave solutions*, *Bull. Math. Biol.*, **57**(3) (1995), 461–486.
10. C. Y. Chung, S. Funamoto, and R. A. Firtel, *Signaling pathways controlling cell polarity and chemotaxis*, *Trends. Biochem. Sci.*, **26**(9) (2001), 557–566.
11. E. J. Crampin, E. A. Gaffney, and P. K. Maini, *Reaction and diffusion on growing domains: Scenarios for robust pattern formation*, *Bull. Math. Biol.*, **61**(6) (1999), 1093–1120.

12. J. C. Dallan and H. G. Othmer, *A discrete cell model with adaptive signalling for aggregation of Dictyostelium discoideum*, *Philos. Trans. Roy. Soc. B*, **352** (1997), 391–417.
13. W. J. Deery and R. H. Gomer, *A putative receptor mediating cell-density sensing in Dictyostelium*, *J. Biol. Chem.*, **274** (1999), 34476–34482.
14. Y. Dolak and T. Hillen, *Cattaneo models for chemotaxis, numerical solution and pattern formation*, *J. Math. Biol.*, **46**(2) (2003), 153–170.
15. B. Ermentrout, *Stripes or spots? nonlinear effects in bifurcation of reaction-diffusion equations on the square*, *Proc. Roy. Soc. Lond. A.*, **434** (1991), 413–417.
16. P. Friedl, S. Borgmann, and E. Bröcker, *Amoeboid leukocyte crawling through extracellular matrix: Lessons from the Dictyostelium paradigm of cell movement*, *J. Leuk. Biol.*, **70** (2001), 491–509.
17. S. F. Gilbert, *Developmental Biology*, Sinauer, Sunderland, Mass., 5th edition, 1998.
18. T. Hillen, *Hyperbolic models for chemosensitive movement*, *Math. Models and Methods in Appl. Sci.*, **12**(7):1007–1034, 2002.
19. T. Hillen and K. J. Painter, *A parabolic model with bounded chemotaxis - prevention of overcrowding*, *Adv. Appl. Math.*, **26** (2001), 280–301.
20. D. Horstmann, *From 1970 until present: The Keller-Segel model in chemotaxis and its consequences I*, *Jahresberichte der DMV*, **105**(3) (2003), 103–165.
21. D. Horstmann, *From 1970 until present: The Keller-Segel model in chemotaxis and its consequences II*, *Jahresberichte der DMV*, 2003. in print.
22. D. Horstmann, K. J. Painter, and H. G. Othmer, *Aggregation under local reinforcement: From lattice to continuum*, *European J. Appl. Math.*, 2003. in print.
23. D. Horstmann and A. Stevens, *A constructive approach to traveling waves in chemotaxis*, *J. Nonlin. Sci.*, 2003. in print.
24. S. Iuchi and L. Weiner, *Cellular and molecular physiology of Escherichia coli in the adaptation to aerobic environments*, *J. Biochem.*, **120**(6) (1996), 1055–1063.
25. E. F. Keller and G. M. Odell, *Necessary and sufficient conditions for chemotactic bands*, *Math. Biosci.*, **27** (1975), 309–317.
26. E. F. Keller and L. A. Segel, *Model for chemotaxis*, *J. Theor. Biology*, **30**:225–234, 1971.
27. E. F. Keller and L. A. Segel, *Travelling bands of chemotactic bacteria: a theoretical analysis*, *J. Theor. Biol.*, **30** (1971), 235–248.
28. S. Kondo and R. Asai, *A reaction-diffusion wave on the skin of the marine angelfish Pomacanthus*, *Nature*, **376** (1995), 675–768.
29. S. G. Kramer, T. Kidd, J. H. Simpson, and C. S. Goodman, *Switching repulsion to attraction: Changing responses to slit during transition in medoderm migration*, *Science*, **292** (2001), 737–740.
30. S. G. Li and K. Muneoka, *Cell migration and chick limb development: Chemotactic action of FGF-4 and the AER*, *Dev. Biol.*, **211**(2) (1999), 335–347.
31. M. J. Lyons and L. G. Harrison, *A class of reaction-diffusion mechanisms which preferentially select striped patterns*, *Chem. Phys. Lett.*, **183** (1991), 158–164.
32. H. Meinhardt, *Models for positional signalling with application to the dorsoventral patterning of insects and segregation into different cell types*, *Development*, supplement:169–180, 1989.
33. M. B. Miller and B. L. Bassler, *Quorum sensing in bacteria*, *Annu. Rev. Microbiol.*, **55** (2001), 165–199.
34. G. L. Ming, H. J. Song, B. Berninger, C. E. Holt, M. Tessier-Lavigne, and M. M. Poo, *CAMP-dependent growth cone guidance by netrin-1*, *Neuron*, **19**(6) (1997), 1225–1235.

35. J. D. Murray, *Nonlinear Differential Equation Models in Biology*, Clarendon Press, 1977.
36. J. D. Murray, *Mathematical Biology*, Springer-Verlag, Berlin, Heidelberg, New York., 1993.
37. T. Nagai and T. Ikeda, *Travelling waves in a chemotactic model*, J. Math. Biol., **30** (1991), 169–184.
38. B. N. Nagorcka, *From stripes to spots: Prepatterns which can be produced in the skin by a reaction-diffusion system*, IMA. J. Math. Appl. Med. Biol., **9** (1992), 249–267.
39. G. M. Odell and E. F. Keller, *Travelling bands of chemotactic bacteria revisited*, J. Theor. Biol., **56** (1976), 243–247.
40. L. Olsen, J. A. Sherratt, P. K. Maini, and F. Arnold, *A mathematical model for the capillary endothelial cell-extracellular matrix interactions in wound-healing angiogenesis*, IMA J. Math. Appl. Med. Biol., **14**(4) (1997), 261–281.
41. H. G. Othmer and A. Stevens, *Aggregation, blowup and collapse: The ABC's of generalized taxis*, SIAM J. Appl. Math., 57::1044–1081, 1997.
42. Q. Ouyang and H. L. Swinney, *Transition from a uniform state to hexagonal and striped turing patterns*, Nature, **352** (1991), 610–612.
43. K. J. Painter, D. Horstmann, and H. G. Othmer, *Localization in lattice and continuum models of reinforced random walks*, Appl. Math. Lett., **16**(3) (2003), 375–381.
44. K. J. Painter, P. K. Maini, and H. G. Othmer, *Complex spatial patterns in a hybrid chemotaxis reaction-diffusion model*, J. Math. Biol., **41**(4) (2000), 285–314.
45. K. J. Painter, H. G. Othmer, and P. K. Maini, *Stripe formation in juvenile *Pomacanthus* via chemotactic response to a reaction-diffusion mechanism*, Proc. Natl. Acad. Sci. USA, **96** (1999), 5549–5554.
46. E. Palsson and H. G. Othmer, *A model for individual and collective cell movement in *Dictyostelium discoideum**, P. Natl. Acad. Sci. USA, **97**(19) (2000), 10448–10453.
47. C. S. Patlak, *Random walk with persistence and external bias*, Bull. Math. Biophys., **15** (1953), 311–338.
48. A. J. Perumpanani, J. A. Sherratt, J. Norbury, and H. M. Byrne, *A two parameter family of travelling waves with a singular barrier arising from the modelling of extracellular matrix mediated cellular invasion*, Physica D, **126** (1999), 145–159.
49. T. J. Poole, E. B. Finkelstein, and C. M. Cox, *The role of FGF and VEGF in angioblast induction during vascular development*, Dev. Dyn., **220** (2001), 1–17.
50. A. Potapov and T. Hillen, *Metastability in chemotaxis models*, J. Dynamics Diff. Eq., 2003. submitted.
51. M. C. Poznansky, I. T. Olszak, B. Foxall, R. H. Evans, A. D. Luster, and D. T. Scadden, *Active movement of T cells away from a chemokine*, Nat. Med., **6**(5) (2000), 543–548.
52. C. Roisin-Bouffay, W. Jang, D. R. Caprette, and R. H. Gomer, *A precise group size in *Dictyostelium* is generated by a cell-counting factor modulating cell-cell adhesion*, Mol. Cell, **6**(4) (2000), 953–959.
53. E. H. Rowsell, J. M. Smith, A. Wolfe, and B. L. Taylor, *CheA, CheW, and CheY are required for chemotaxis to oxygen and sugars of the phosphotransferase system in *Escherichia coli**, J. Bacteriol., **177**(20) (1995), 6011–4.
54. E. G. Ruby, *Lessons from a cooperative, bacterial-animal association: the vibrio fischeri-euprymna scolopes light organ symbiosis*, Annu. Rev. Microbiol., **50** (1996), 591–624.
55. L. Segel, *A theoretical study of receptor mechanisms in bacterial chemotaxis*, SIAM J. Appl. Math., **32** (1977), 653–665.

56. J. A. Shapiro, *Thinking about bacterial populations as multicellular organisms*, *Annu. Rev. Microbiol.*, **52** (1998), 81–104.
57. J. A. Shapiro and M. Dworkin, editors, *Bacteria as Multicellular Organisms*, Oxford University Press, Oxford, New York., 1997.
58. H. J. Song, G. L. Ming, Z. G. He, M. Lehmann, L. McKerracher, M. Tessier-Lavigne, and M. M. Poo, *Conversion of neuronal growth cone responses from repulsion to attraction by cyclic nucleotides*, *Science*, **281**(5382) (1998), 1515–1518.
59. H. J. Song and M. M. Poo, *The cell biology of neuronal navigation*, *Nature Cell Biology*, **3**(3) (2001), 81–88.
60. X. Sun and M. Ward, *Dynamics and coarsening of interfaces for the viscous Cahn-Hilliard equation in one spatial dimension*, *Studies Appl. Math.*, **105** (2000), 203–234.
61. A. M. Turing, *The chemical basis for morphogenesis*, *Phil. Trans. Roy. Soc. Lond. B*, **237** (1952), 37–72.
62. R. Tyson, S. R. Lubkin, and J. D. Murray, *A minimal mechanism for bacterial pattern formation*, *P. Roy. Soc. Lond. B Bio.*, **266** (1999), 299–304.
63. R. Tyson, S. R. Lubkin, and J. D. Murray, *Model and analysis of chemotactic bacterial patterns in a liquid medium*, *J. Math. Biol.*, **38**(4) (1999), 359–375.
64. D. E. Woodward, R. Tyson, M. R. Myerscough, J. D. Murray, E. O. Budrene, and H. C. Berg, *Spatiotemporal patterns generated by Salmonella typhimurium*, *Biophys.J.*, **68**(5) (1995), 2181–2189.
65. X. S. Yang, D. Dormann, and A. E. Munsterberg and C. J. Weijer, *Cell movement patterns during gastrulation in the chick are controlled by chemotaxis mediated by positive and negative FGF4 and FGF8*, *Dev. Cell*, **3**(3) (2002), 425–437.
66. I. B. Zhulin, E. H. Rowsell, M. S. Johnson, and B. L. Taylor, *Glycerol elicits energy taxis of Escherichia coli and Salmonella typhimurium*, *J. Bacteriol.*, **179**(10) (1997), 3196–3201.

DEPARTMENT OF MATHEMATICS, HERIOT-WATT UNIVERSITY, EDINBURGH
EH14 4AS, UK

E-mail address: painter@ma.hw.ac.uk

DEPARTMENT OF MATHEMATICAL AND STATISTICAL SCIENCES, UNIVERSITY OF
ALBERTA, EDMONTON T6G 2G1, CANADA,

E-mail address: thillen@ualberta.ca